SOLAR-POWERED ESS MESH NETWORKS

Design and Resource Allocation for Solar-Powered ESS Mesh Networks

By
Amin Farbod, B.Sc.

A Thesis
Submitted to the School of Graduate Studies
in partial fulfilment of the requirements for the degree of

M. A. Sc.
Department of Electrical and Computer Engineering
McMaster University

MASTER OF APPLIED SCIENCE (2005) McMaster University
(Electrical and Computer Engineering) Hamilton, Ontario

TITLE:
Design and Resource Allocation for Solar-Powered ESS Mesh Networks

AUTHOR: Amin Farbod, B.Sc.
(Isfahan University of Technology , Iran)

SUPERVISOR: Dr. Terence D. Todd and Dr. Ted Szymanski

NUMBER OF PAGES: xiii, 97

Abstract

In this thesis we consider design methodology and resource allocation for IEEE 802.11 ESS mesh networks. In such networks, solar powered access points can be used to significantly reduce the installation cost of outdoor WLAN hotzones. SolarMESH is a network of this kind and is currently in its second year of an operational deployment. In SolarMESH, the cost of the solar panel/battery can be a significant fraction of the total, and therefore reducing AP power consumption is very important. Unfortunately, access point power saving is not currently supported under IEEE 802.11, but this would be very useful in future versions of the standard. A design methodology is presented for sustainable solar powered ESS mesh networks, assuming a power saving version of IEEE 802.11. First, a load profile for each network node is determined. The load profile is a time function which represents the average workload for which the node in question is designed. For a given geographic location, public meteorological data is then used together with the averaged offered capacity profile to provision each node subject to a target outage probability.

The design is statistical since future load conditions and solar insolation may not exactly match that for which the node was designed. For this reason, a control algorithm is introduced which attempts to maintain outage-free operation of the node by introducing a capacity deficit under certain conditions.

Results are presented showing that significant resource reductions are possible using the proposed resource allocation methodology. The results also give a strong motivation for including access point power saving in outdoor ESS mesh networks.

Acknowledgements

I would like to express my sincere thanks to my supervisors, Dr. Terence D. Todd and Dr. Ted Szymanski for their guidance and support throughout my graduate studies at McMaster University. Working under their supervision has been a great chance for me to learn a lot in both academic and non-academic areas. Indeed, their consistent help and support made it possible for me to finish this work.

I am grateful to Dr. Dongmei Zhao and Dr. Nicola Nicolici, for reviewing my thesis, and for their valuable suggestions and comments. Also, I would like to thank all the members of the Wireless Networking Group, for their helpful discussions.

Finally, I would like to give my special thanks to my parents and my brother, for their encouragement and support.

Contents

List of Figures

List of Tables

Glossary

ACK

Acknowledgement. Notification data sent from one network station to another to acknowledge the proper reception of some data(for example, the receipt of a frame).

AP

Access Point; A device that serves as a communications gateway for wireless clients and provides a connection to a wired LAN.

CSMA

Carrier Sense Multiple Access - A medium access control technique for media shared among multiple transmitting stations. A station that wants to transmit first senses the medium and transmits only if the medium is idle.

Diffuse Irradiation

Diffuse Solar radiation is caused by diffraction through the sky and consists of non-direct radiation components.

Direct Radiation

Radiation beams coming directly from the sun, as opposed to diffuse radiation.

EDCA

Enhanced Distributed Channel Access; An extension to the exponential back-off algorithms used to arbitrate channel access between different contending wireless stations.

ESS Mesh

An ESS Mesh is a set of Access Points (APs) interconnected with wireless links.

FPS

Forced Power Saving; Technique used in this thesis to save power in APs by artificially reducing the capacity offered by the AP.

HCCA

HCF controlled channel access; An extension to the Point Coordination Function(PCF) that supports QoS

HotSpot

A WiFi wireless access point in a public place such as an airport, university campus or train station.

LAN

Local Area Network: a local computer network for communication between computers; specifically a technology connecting computers, file sharing and printing services in a building.

MAC

Media Access Control. A sublayer of the datalink layer in the ISO network reference model that defines protocols needed to control shared media among multiple transmitting stations.

PoE

Power-over-Ethernet; A method to provide APs with electrical power over Ethernet. Using Power-over-Ethernet a single Ethernet cable can be used to carry both power and data to each device.

PSAP

Power Saving Access Point; An AP that uses power saving techniques to reduce its power consumption.

PV

Photovoltaic; Electrical energy in photovoltaic systems is generated from light.

WDS

Wireless Distribution System is a type of distribution system used to interconnect APs that includes some wireless links.

WiFi

Wi-Fi, short for Wireless Fidelity, is a set of standards for WLANs currently based on the IEEE 802.11 specifications.

WLAN

A Wireless Local Area Network (WLAN) is similar to a LAN, except that data transmission is done over a wireless medium.

Chapter 1

Introduction

1.1 Overview

The dependence of the modern life on ubiquitous communications and information services is rapidly increasing, and wired networking can no longer satisfy new applications. In contrast to wired communications, Wireless Communications provides more flexibility and supports mobility. In recent years wireless communication has witnessed some major progresses in both the industrial and research directions. In the academic environment, Wireless Communication as a challenging problem has received lots of research interest. This is mainly due to the scarce amount of bandwidth available to wireless devices and the shared nature of the wireless medium which make the support of the data communications services more difficult when compared to wired networks.

One of the most successful Wireless Local Area Network (WLAN) standards

is the IEEE 802.11 family defined by the Institute of Electrical and Electronics Engineers (IEEE). Wireless LANs are an extension to the concept of the Local Area Network (LAN) which has been in use for a long time. LANs were originally limited to wired networks. With the introduction of IEEE 802.11, the concept of the LAN was extended to include the wireless medium. In WLANs no wired connection is necessary which makes it possible to support mobile networking devices.

Although a few alternatives exist, currently IEEE 802.11 is the most widely used protocol in manufactured products. IEEE 802.11 specifies the protocol details at both the Medium Access Control (MAC) and the physical layer. IEEE 802.11 includes several substandards. IEEE 802.11a,b,g are the major protocol specifications which differ mostly on the frequency band and the type of modulation employed. This results in differences in the available bandwidth to the users. IEEE 802.11a operates at 5GHz and is based on Orthogonal Frequency Division Multiplexing (OFDM). IEEE 802.11b operates within the 2.4 GHz band and uses Direct Sequence Spread Spectrum (DSSS) in the physical layer. Although 802.11a can support up to 54 Mbps, 802.11b only provides data rates of 1 Mbps, 2 Mbps, 5 Mbps and 11 Mbps. IEEE 802.11g is an extension of 802.11b which again uses the 2.4 GHz band but with the use of two modulation techniques it can offer up to 54 Mbps.

Along with the advances in WLAN technologies, the variety of applications supported on mobile wireless devices is increasing on a daily basis. This has resulted in greater demands for extending wireless coverage areas and supporting traffic hot-spots. Currently, multi-hop communications is being used

for coverage extension and wireless distribution between IEEE 802.11 access points (APs). These networks are being standardized under IEEE 802.11s ESS mesh [15], which intends to promote interoperability between different vendor solutions. ESS mesh networks provide IEEE 802.11 coverage for mobile stations (MSs) and also perform wireless distribution (WDS) using multihop relaying between mesh APs (MAPs) and mesh points (MPs).

1.2 Contributions of This Thesis

One of the major costs of ESS mesh deployment is that of providing MAPs/MPs with electrical power and wired network connections. Although power can be supplied through Power Over Ethernet (POE), such a solution requires a wired network connection, which is often expensive due to increased installation time and cost in outdoor ESS mesh deployments. Also, if multi-hop communication is used there is no need to provide mesh APs with wired network connections since the the multi-hop wireless distribution system can be used to relay packets. One possible solution to this problem is to use battery powered APs and to equip them with receivers of renewable energy sources such as solar power or wind power.

For the past several years, the SolarMESH network has been under development and undergoing deployment trials at McMaster University [1]. In SolarMESH, the mesh APs are solar powered and completely tetherless, and can be deployed quickly and inexpensively for outdoor WiFi coverage in campuses, building complexes and other WiFi hotzones.

In the design of solar-powered ESS mesh networks several problems must be considered. In such a network, the cost of the solar panel and battery can be a significant fraction of the total. For this reason it is important to minimize access point power consumption as much as possible. Also, the resource allocation must be done accurately to avoid under/over estimation in the amount of the resources required to achieve a certain level of network performance and reliability.

In our results we show the significant node resource reductions which are possible when power saving techniques are employed in APs . Unfortunately, IEEE 802.11 does not include any native procedures that would allow for AP power saving. In [50] several protocols were proposed which can achieve some degree of mesh AP power saving in cases where legacy end stations are being accommodated. Unfortunately, there are many practical disadvantages to these procedures, mainly caused by IEEE 802.11's assumption that an AP is always active on its assigned channel. This aspect of IEEE 802.11 is a major impediment to the development of real power saving WLAN infrastructure.

In this thesis we consider resource allocation and design methodology in solar powered ESS mesh networks. A design methodology is presented for solar powered ESS mesh networks, assuming a power saving version of IEEE 802.11. First, a load profile for each network node is determined. For a given geographic location, public meteorological data is then used to design the node subject to a target outage probability. The design is statistical since future load conditions and solar insolation may not exactly match that for which the node was designed. For this reason, a control algorithm is introduced

which attempts to maintain outage-free operation of the node by introducing a capacity deficit under certain conditions. Results are presented showing that significant resource reductions are possible using the proposed design. The results also give a strong motivation for including access point power saving in outdoor ESS mesh networks.

1.3 Related Work

1.3.1 ESS Mesh Networking and IEEE 802.11 Wireless Infrastructure

Wireless mesh networking (WMN) is a very active area, and many systems have recently been proposed and constructed. Interest in Wireless Mesh Networking is continually increasing and there are many applications and possibilities in this field not explored yet. Wireless Mesh networks can be divided into two main categories, those based on community area networks, and those based on ESS mesh networks. In community networks the nodes that form the multihop relaying infrastructure are typically also the end wireless nodes. There are many examples of this type of network such as MIT Roofnet [27], Seattle Wireless [43] , the San Francisco BAWUG [41] and the Southampton Open Wireless Network [45]. In [47], a wireless community network built in the Netherlands and the technical challenges in its planning are discussed.

ESS mesh networks are different in that they are hierarchical, i.e., the mul-

tihop relaying occurs between access points and is done to support communications between end user nodes that are associated with the access points. In an IEEE 802.11 ESS mesh, mesh APs (MAPs) provide both coverage for end user stations but also relay traffic to other MAPs and mesh points (MPs). A mesh point is a relay node that does not provide coverage for end user stations [15]. There are many examples of ESS mesh products that have recently been introduced [5, 25, 26, 33]

Since wireless mesh networking is fairly new, not many theoretical research studies have been done on the topic. Sichitiu[18], is among one of the first theoretical work on mesh networking. In this paper, the concept of the bottleneck collision domain is presented which is basically the geographical area with the worst collision condition. In the bottleneck collision domain the largest number of transmitting stations will be contending to access the channel. Based on this concept, the nominal capacity of WMNs can be estimated. In their method, it is assumed that a mechanism to enforce absolute fairness is employed at the MAC layer. They show that in WMNs the throughput decreases as $O(1/n)$, with an increase in n; the number of nodes in the network. This is true because all the traffic load passes through the gateway node.

In [28] and [29], some interesting measurement results of real-world hot-spot traffic statistics are presented. Traffic throughput graphs for a one-week period are obtained. It is reflected in the results that the traffic load variations are approximately periodic. We will consider this fact later when we are evaluating the performance of the solar-powered mesh nodes.

1.3.2 Energy Issues in Networking

Energy limitation issues in networking have been raised since the introduction of portable devices, and work on this topic has evolved to include many different types of networking scenarios, such as wireless LANs, ad hoc networks, and sensor networks. In [17], power conservation techniques at different layers of the wireless network protocol stack are studied. Also, energy efficiency issues in ad hoc networks are reviewed in [11].

In [10], traffic shaping methods to increase the effective battery capacity by exploiting the charge recovery effect in batteries are presented. Charge recovery effects occur when batteries are used under bursty or pulsed loads. It is known that the performance of energy conversion in a battery is higher when the discharge current is abrupt and bursty rather than continuous and fixed.

In the context of ad-hoc networks, energy and power aware routing algorithms have received a great deal of research focus. In [44], five different routing metrics to increase the energy efficiency and service reliability of ad-hoc wireless networks are proposed, and their trade-offs are discussed. In [46], it is shown that there exists a trade off between the first node failure time and the total network lifetime, i.e., we can not optimize both of them simultaneously. A power-aware routing algorithm capable of balancing between these two goals is proposed.

Energy management issues in sensor networks have also received a serious consideration recently. In sensor networks, energy resources are very limited making it essential to consider the network lifetime as a significant constraint of the system. In [19], a framework to extend network lifetime by extracting

environmental energy is proposed. There, it is assumed that nodes would have access to some energy sources, while the distribution of this energy might not be homogeneous everywhere. They propose an adaptive framework for learning the energy environment and some algorithms to use this information in assigning tasks to different nodes.

In infrastructure-based networks such as IEEE 802.11, the issues of power saving have mainly dealt with end user stations, since access points and base-stations are normally assumed to have wired AC power connections. In a solar-powered ESS mesh, the MAPs and MPs are photovoltaic (PV) systems which provide reliable operation by achieving a sustainable balance between energy input and output. For this reason, power consumption on the MAPs and MPs is very important. In the next chapters, this issue will be considered closely.

1.3.3 Solar Powered Communication Systems and Networks

Solar energy has been used in communication systems for many decades, and its application now ranges from powering telephone systems to operating emergency message centers in rural areas. In addition to its use in communications, solar power is also used in places where either grid power is not present or alternative energy sources are required.

Several projects have used solar energy to power IEEE 802.11 relays into otherwise inaccessible areas [14]. In [49, 48] and [42] solar power is used in a

wireless sensor network. Some nodes will be in a position to receive more solar energy than others and thus they are better equipped to perform functions such as packet forwarding. In this study energy-aware routing algorithms were used to favor such nodes. In [24] solar powered wireless detectors are used in an urban traffic information collection system. To our knowledge however, there is no literature which deals with sustainable solar-based power saving ESS mesh infrastructure.

Due to the motion of the earth, solar insolation experiences daily and yearly cyclic behavior. These variations have a strong deterministic component but processes such as air humidity, pressure and cloud cover induce randomness into the received insolation. The modelling of the above processes are mainly done using stochastic processes because they are too complicated to be studied using deterministic models. Due to the importance of this issue solar radiation models will be discussed in the next chapter.

A problem extensively studied in the literature is the sizing of photovoltaic systems, i.e., determining the required solar-panel and battery size to achieve a desired performance level. Different sizing methods and their accuracy are studied in [30] along with discussions of how various PV components result in different system configurations. Three probabilistic methods for sizing PV systems are compared in [23]. The first method sizes the battery so that it can support a fixed load for a set number of days. Similarly, the panel is sized so that a full battery re-charge can be done within a specified time period. The second scheme is based on detailed computer simulations. The last approach is based on Markov chain modelling of the battery state-of-charge. It has been

shown that the second method yields by far the most accurate results [23] and this is the method we adopt in this thesis.

In [9] a Markov chain model was used for battery state of charge in PV systems. To use this approach however, the variance and mean of the daily solar insolation must be known. This model was refined in [8] and includes the effects of inter-daily correlations in solar irradiation. Another performance evaluation of PV systems based on Markov chain modelling is presented in [39]. Another closed form solution for PV system sizing is studied in [3].

In [3] and [13] the sky clearance index is used for simulation of solar irradiance. Reference [6] considers the optimum PV array sizing for a stand-alone hybrid wind/PV system. In [38] variable loading is taken into account in the sizing of PV systems. A fuzzy decision-making process is used in [22] to evaluate subjective factors in the PV system sizing decision. Energy management issues in space station, when there are several tasks to perform under limited energy constraints is considered in [7]. A penalty function is used in making rescheduling decisions.

Much of the quoted work assumes idealized battery models which can lead to significant inaccuracies. In practical PV systems for example, battery capacity is a strong function of the ambient temperature. In [4, 40] and [37] some relevant models for the battery behavior are studied.

In most of the quoted work on stand-alone PV system sizing it is assumed that solar insolation statistics are daily and yearly cyclostationary. This implies that a design passed on enough past data will be valid for the future. However, it has been reported that this may not be the case [30]. The effect of global

warming on the design of stand-alone PV systems is studied in [12].

1.4 Structure of This Thesis

The rest of the thesis is organized as follows.

Chapter 1 briefly introduces the WLAN background as well as the motivation and contributions of this thesis.

Chapter 2 introduces the solar radiation data and models used in this thesis.

Chapter 3 introduces the current IEEE 802.11 standard. ESS mesh networking and the power saving access point infrastructure are explained.

Chapter 4 describes the proposed PSAP design methodology. The concept of capacity profile is introduced which is used in characterizing AP traffic loading.

Chapter 5 introduces the outage control algorithms which can be used to improve the outage performance of a solar-powered mesh AP.

Chapter 6 presents the performance results and the simulation experiments conducted to evaluate the proposed design methodology and control schemes.

Chapter 7 summarizes the work and proposes some future research topics.

Chapter 2

Solar Radiation Data and Models

2.1 Overview

In order to evaluate the performance of a PV system, knowledge of the solar radiation is required. Theoretically, it is impossible to know in advance how much solar energy would be received at the solar panel of a PV system. However, assuming cyclo-stationary recurrence of weather conditions, records of the past solar irradiations can be used to determine the performance of PV systems.

Public meteorological data can be used for this purpose. Generally, the measurements are done for some specific standard conditions such as irradiance

on a horizontal plane. In practice, depending on the site-specific situation the panel may be tilted toward the equator or it might be positioned even more vertical to avoid the accumulation of snow during the winter. To be able to use public meteorological data in these situations some conversion methods are required to estimate the received solar energy at an arbitrarily positioned panel based on standard measurements of the solar irradiation on a horizontal and a fully-tracking (direct normal) panel.

In this chapter, the two sources of meteorological data for North America are introduced and we explain the types of available solar data from each of them. We then take a closer look at solar radiation models, which help us to convert the available solar radiation measurements to useful information for simulation purposes. Finally, the procedure we used to estimate the total received solar energy at an arbitrary positioned panel is explained.

2.2 Solar Radiation Records

The results in this thesis use solar irradiation data from two different North American sources. Data for many locations in the United States is available from the National Solar Radiation Data Base (NSRDB), National Renewable Energy Laboratory (NREL), U.S. Department of Energy [32]. In Canada, data may be obtained from the National Climate Data and Information Archive, The Meteorological Service of Canada (MSC) [31]. The NREL data provides insolation records including global horizontal solar irradiance, direct normal solar irradiance and diffuse horizontal solar irradiance for each hour from Jan-

uary 1, 1961 through December 31, 1990 for 239 different sites. Later we will describe the meaning of each of these terms. The NSRDB contains a total of 56 Primary and 183 Secondary stations. When a station contains only modelled solar radiation data, it is referred to as a Secondary station while in primary stations if not all at least some parts of of the data are obtained using real measurements. In addition to the fields mentioned above, to assist in using solar conversion models, two other fields are also included in the hourly records; Extraterrestrial Horizontal Radiation and Extraterrestrial Direct Normal Radiation. The MSC records contain similar data for 148 Canadian locations. These files, in addition to the traditional fields contain temperature, sky condition, station pressure records, etc. The history for the Canadian sites is not exactly the same, but for most locations data is available from 1953 to 2001.

2.2.1 Solar Radiation Data Fields

Five different solar irradiation fields are used from the data in both of the American and Canadian sites. These are listed as follows.

1. Extraterrestrial Horizontal Radiation

   This is the amount of solar radiation received on a horizontal surface at the top of the atmosphere.

2. Extraterrestrial Direct Normal Radiation

   This is the level of solar radiation received on a surface normal to the sun at the top of the atmosphere.

3. Global Horizontal Radiation

   The total amount of direct and diffuse solar radiation received on a horizontal surface.

4. Direct Normal Radiation

   This is the amount of solar radiation received directly from the sun within a field of view centered on the sun

5. Diffuse Horizontal Radiation

   The level of solar radiation received from the sky (excluding the solar disk) on a horizontal surface.

The first two fields are deterministic and can be calculated using the sun-earth distance and position equations, but the rest of the fields are random processes. In fact, due to the earth motion around the sun and the rotation of the earth around its axis, solar insolation experiences cyclic changes over the year and these variations are deterministic to a large extent, however, some complex weather processes such as humidity, air pressure and cloud type cover affect the received insolation.

2.3 Solar Radiation Conversion Model

In most of the photovoltaic (PV) applications, fixed panels are pointed directly south and sloped slightly greater than the geographic latitude so that solar absorption is highest during winter months. Meteorological data however, is only available for horizontal and fully-tracking (direct normal) components

and cannot be used directly for a fixed planar solar panel. For this reason a conversion model is used to compute the energy incident on the panel using horizontal and fully-tracking irradiance records. The total energy received by a solar panel consists of three components as follows.

1. Direct radiation I_c

   Radiation beams coming directly from the sun.

2. Diffuse radiation D_c

   This is caused by diffraction through the sky and consists of non-direct radiation components.

3. Ground-Reflected radiation R_c

   This is the result of components that reflect from the ground plane and impinge on the solar panel

The total solar irradiation on the panel is therefore,

$$G_c = I_c + D_c + R_c. \tag{2.1}$$

The direct component calculation is a straightforward problem. The diffuse component estimation requires a more complex model. Several attempts have been made previously in the literature to propose a more accurate model for this component. Later, we will describe the most widely used and accepted method for the diffuse component calculation.

The ground-reflected component is not considered in this thesis since it is highly site-dependent and detailed knowledge of the "surrounding ground albedo" is required [36]. Typically this component is a small fraction of the

total and does not significantly contribute to total solar insolation. However, when it is not considered the results we obtain can be considered to be a worst-case underestimation. This is a reasonable practical design approach.

2.3.1 Solar Angles

In addition to the solar radiation intensity, the angle of incidence determines the energy received by the panel. This angle is a function of the time of day and day of the year. In this section, we explain the different parameters and angles involved and how they are used to calculate the amount of solar radiation on a tilted plane.

The angle at which the solar radiation strikes the panel is called the incidence angle (θ). This angle is mainly a function of the position of the sun in the sky, and the slope and orientation of the panel. These two factors are specified using several parameters which are briefly described below.

1. Solar Declination Angle (δ)

   This is the angle between a plane perpendicular to incoming solar radiation and the rotational axis of the earth. It can be calculated as follows [20]

   $$\delta = 23.45^\circ \cdot sin[360(284 + n)/365], \tag{2.2}$$

   where n is the Julian day.

2. Hour Angle

The Hour Angle is the angular distance that the earth has rotated in a day. It is equal to 15 degrees multiplied by the number of hours from local solar noon and can be expressed as,

$$h = 15 \cdot (t_s - 12) \tag{2.3}$$

3. Zenith Angle

   This is the angle which is formed between the solar radiation beam and a vertical line at the panel location. It can be computed as follows,

$$cos(\theta_z) = sin(\phi)sin(\delta) + cos(\phi)cos(\delta)cos(h). \tag{2.4}$$

These different parameters are shown in Figure 2.1.

2.3.2 Direct Solar Radiation

The direct component of solar radiation on a tilted plane is a function of the direct normal solar radiation and the incidence angle. In [2], for an inclined plane facing toward equator the incidence angle is given as

$$cos(\theta) = cos(\phi - \beta)cos(h)cos(\delta) + sin(\phi - \beta)sin(\delta) \tag{2.5}$$

This can be simplified further for the case where the tilt angle is equal to the value of the latitude,

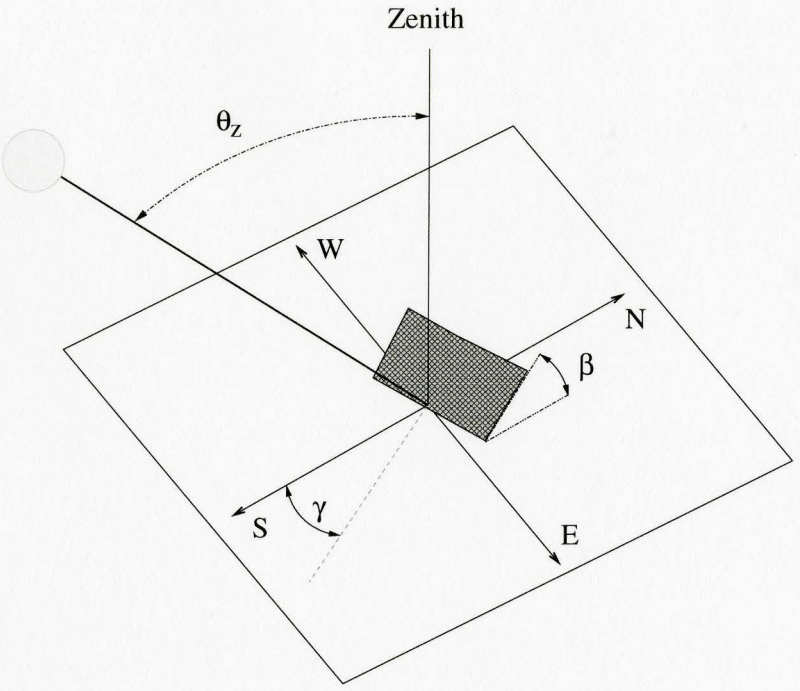

Figure 2.1: Solar Angles

$$cos(\theta) = cos(h)cos(\delta). \tag{2.6}$$

This means that the solar incidence angle for an equator-facing plane is only a function of the hour angle and the declination angle. Now, the direct component of solar radiation can be written as

$$I_c = I \cdot max[0, cos(\theta)]. \tag{2.7}$$

The reason that we are taking the maximum of zero and $cos(\theta)$ is that during the night when sunlight is unavailable, the unmodified equation is not

correct.

2.3.3 Diffuse Solar Radiation

In addition to the direct radiations from the sun, another type of radiation is also received at a solar panel which is caused by diffraction through the sky. This radiation does not come directly from the sun and its strength is a function of sky clearness and brightness. We now describe the widely accepted Perez model for estimation of the diffuse component of solar irradiance on tilted planes[36]. This model has been extensively verified and yields the most accurate results.

In the primitive models, a simple isotropic distribution of radiance throughout the sky dome has been assumed. Further refinements have incorporated the observed directionality of diffuse radiation [36]. In [34], estimations were improved by introducing a simple representation of the sky dome, and circumsolar and horizon anisotropy factors, $F_1$and F_2. In this model the diffuse radiation is described by an isotropic background, similar to previous models, but it also includes two regions of enhanced radiation, i.e.,

1. A disk of variable size around the sun, represented by F_1 which is a multiplier for circumsolar region (See Figure 2.2), and,

2. a horizontal band of variable height at the horizon, represented by F_2 which is a multiplier for the horizon region (See Figure 2.2)

F_1 and F_2 are a function of the sky condition and have been reported to be consistent from site to site [34]. In this model, two parameters ϵ (sky clearness)

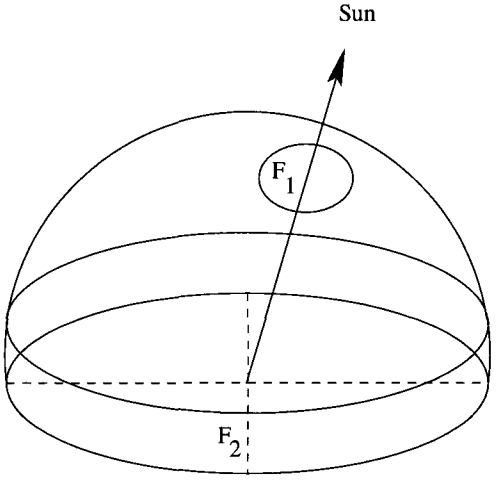

Figure 2.2: Representation of the sky dome model used in [35]

and Δ(sky brightness) are used to characterize the condition of the sky. ϵ which is used as a measure of sky's clearness is given in [34] as follows,

$$\epsilon = [(D_h + I)/D_h + \kappa\theta_z^3]/[1 + \kappa\theta_z^3], \tag{2.8}$$

where κ is assumed to be 1.041 for θ_z in radians. Furthermore, ϵ values are discretized [34] to eight different levels ranging from 1 (overcast) to 8 (clear sky). The mapping table is given in table 1 [34]. In Equation 2 of [34], Δ is given as a measure of the sky's brightness,i.e.,

$$\Delta = D_h \cdot m/I_0, \tag{2.9}$$

where m can be obtained from ref. 11 of [34]. The F_1 and F_2 values can be obtained by looking up Table 6 in [34] where a set of coefficients are chosen based on the category into which the current sky's clearness index ϵ falls. This

table of coefficients, as described in [34], is the result of experimental work in which it has been attempted to adjust coefficients so that RMS and mean bias error for all sites studied are minimized. Here, error refers to the difference between the actual solar diffuse insolation records and what the model has yielded.

Finally, the diffuse component on tilted plane ([34], Equation 9) is given as follows,

$$D_c = D_h[(1 - F_1)(1 + cos\beta)/2 + F_1 a/b + F_2 Sin\beta], \tag{2.10}$$

where a=max(0,cosθ) and b=max(0.087, $cos(\theta_z)$). As described, the three different parts of the above equation are specifying the the isotropic diffuse radiation from the sky dome, the radiations originated from the circumsolar region and those originated from the horizon region.

2.4 Conversion Algorithm

In this section the algorithm we used to convert the available solar radiation measurements to useful information for simulation purposes is explained. We will follow a step-by-step approach to calculate the total irradiance on a tilted plane, which is the sum of the direct and diffuse components.

Steps:

1. Estimation of the direct component

$$I_c = I \cdot max(o, cos\theta), \tag{2.11}$$

where θ is computed using the Equation (4a) from [2],

$$cos\theta = cos(\phi - \theta_s)cos(h)cos(\delta) + sin(\phi - \theta_s)sin(\delta) \tag{2.12}$$

2. δ is calculated using eq. 4 from [20],

$$\delta = 23.45° \cdot sin[360(284 + n)/365], \tag{2.13}$$

3. h, or hour angle is estimated according to the below formula,

$$h = 15 \cdot (t_s - 12) \tag{2.14}$$

4. Zenith Angle Calculation

$$cos(Z) = sin(\phi)sin(\delta) + cos(\phi)cos(\delta)cos(h) \tag{2.15}$$

5. Calculation of ϵ

$$\epsilon = [(D_h + I)/D_h + \kappa Z^3]/[1 + \kappa Z^3] \tag{2.16}$$

and κ is assumed to be 1.041 for Z in radians.

6. Calculation of Δ

$$\Delta = D_h.m/I_0, \tag{2.17}$$

where m can be obtained using the ref. 11 of [34], $m = \frac{1}{cosZ+a(b-z)^{-c}}$ and we have a=0.50572, b=6.07995, c=1.6364.

7. ϵ category

   ϵ values are discretized to 8 different categories ranging from 1 (overcast) to 6.5 (clear sky)

   Epsilon Categories = (1, 1.065 , 1.230 , 1.500 , 1.950 , 2.800 , 4.500 , 6.200);

8. Diffuse component on tilted plane ([34], Equation 9)

$$D_c = D_h[(1 - F_1)(1 - cos\theta_s)/2 + F_1 a/b + F_2 Sin\theta_s, \tag{2.18}$$

   where $a = max(0, cos\theta)$ and $b = max(0.087, cosZ)$.

9. Estimation of F_1 and F_2

   F_1 and F_2 are calculated based on the coefficients given in Table 6 in [34].

   Perez Coefficients = (

   [-0.008 , 0.588 ,-0.062 ,-0.060 , 0.072 ,-0.022],

   [0.130 , 0.683 ,-0.151 ,-0.019 , 0.066 ,-0.029],

   [0.330 , 0.487 ,-0.221 , 0.055 ,-0.064 ,-0.026],

   [0.568 , 0.187 ,-0.295 , 0.109 ,-0.152 ,-0.014],

[0.873 ,-0.392 ,-0.362 , 0.226 ,-0.462 ,-0.001],

[1.132 ,-1.237 ,-0.412 , 0.288 ,-0.823 , 0.056],

[1.060 ,-1.600 ,-0.359 , 0.264 ,-1.127 , 0.131],

[0.678 ,-0.327 ,-0.250 , 0.156 ,-1.377 , 0.251])

10. The total irradiance on a tilted plane would be the sum of the results of step 1 and 8

    $G_c = I_c + D_c$

Nomenclature:

ϕ = Location's Latitude

β = Plane Slope

θ = Incidence Angle

γ = Plane Azimuth Angle

h = Hour Angle

t_s = Solar Time

n = Julian Day (1 ... 365)

ϵ = Sky's Clearness

Δ = Sky's Brightness

θ_z =Zenith Angle

m = Relative Optical Airmass

D_h = Horizontal Diffuse Irradiance

I = Direct normal Irradiance

I_0 = Extraterrestrial Irradiance

I_c = Direct Irradiance on tilted plane

D_c = Diffuse Irradiance on tilted plane

G_c = Total Irradiance on tilted plane

Chapter 3

IEEE 802.11 and Power Saving Access Point Infrastructure

3.1 Overview

The IEEE 802.11 standard is the main underlying protocol architecture considered in this thesis. IEEE 802.11 provides some methods for power saving at the end stations. Power saving functionality for end stations results in a scale down of the required battery size in wireless mobile devices. This, in turn, means less weight, longer battery life and more flexibility and portability.

The recent demands for wireless mesh networking has resulted in the need to sometimes deploy wireless APs in inaccessible places where the electrical power grid is not available. In SolarMesh networks, solar power is used to

solve this problem and to make the widespread deployment of wireless mesh APs easier. However, the resource requirements and the energy provisioning of these solar-powered nodes depends on the APs power consumption which was not originally a concern to the designers of the IEEE 802.11 standard.

Two variations of IEEE 802.11 supporting AP power saving have recently been proposed by the Wireless Networking Research Group at McMaster University [21, 50]. In the first one the power saving uses fixed sleep and operation periods. In the most recent one, a dynamic approach has been proposed where the AP adaptively modifies its sleep schedule to be able to support the current load and to be saving as much power as possible. These schemes play a major role in the core of our outage control algorithms. Also, the proposed resource allocation and design methodology for solar-powered PSAPs are influenced by these schemes.

In this chapter, we briefly overview the IEEE 802.11 architecture. The standard method in IEEE 802.11 for power saving at the end stations is explained. Then the ESS mesh networking and IEEE 802.11s substandard are explained. Finally a power saving ESS mesh infrastructure is described.

3.2 IEEE 802.11 Standard

The IEEE 802.11 standard address wireless networking applications with a range of about 100-200 meters for outdoor and indoor situations. It specifies protocol details for the MAC sublayer and the Physical layer.

When the communication media is shared among different users, channel

contention may occur. The purpose of the MAC layer is to arbitrate access to the channel between users. When more than one user transmit, their signals may interfere. The MAC layer protocol provides methods to resolve this contention.

IEEE 802.11 supports two types of channel control algorithms at the MAC sublayer. The first, Distributed Coordination Function (DCF) is a distributed scheme where the arbitration decision is made using a distributed random algorithm called exponential back-off. The other one, Point Coordination Function (PCF), is a centralized algorithm where the AP grants transmission opportunities to end stations basad on a polling mechanism. While DCF is the fundamental access mechanism and it is mandatory, PCF is optional and is not supported in some devices.

DCF is based on the Carrier Sense Multiple Access with Collision Avoidance (CSMA/CA) mechanism. Collision detection as it is done in Ethernet (Wired LANs) is not possible in wireless networks, for several reasons. First of all, a wireless device can not receive other signals when it is transmitting because its own signal strength in that frequency band is orders of magnitude higher than those of the other transmitters. Also, in wireless communications the propagation range of the signals from transmitters located at different places is not equal, a collision free transmission at the sender is not necessarily equal to an interference-free reception at the destination. In IEEE 802.11 an ACK frame for acknowledgement is used to confirm a successful reception. If the ACK is not received at the sender following a frame transmission, the frame is retransmitted again by the sender.

In DCF before transmission, a station senses the channel to check if it is busy. If the channel is idle the station sends its data frame. If the channel is busy the station chooses a random number as a back-off time which determines for how long the station has to wait before trying to transmit the data frame again. The back-off counter is deceased over the time whenever the channel is sensed idle.

The other access mechanism, PCF, is based on polling. Since PCF resolves contention based on a centralized approach it can provide a contention-free frame transfer service. In 802.11, service advertisements called beacons, are periodically broadcast by the AP. The time period between transmissions of successive beacons is called a superframe. PCF divides every superframe into two parts, a contention-free period (CFP) and a contention period (CP). In the CFP, the AP polls waiting end stations and grants them a transmission opportunity. This period is followed by a mandatory CP during which stations contend to access the channel based on the DCF access mechanism. The support of this CP is mandatory for all wireless devices working in PCF mode to make the simultaneous co-existence of the DCF and PCF schemes in the same service area possible.

3.2.1 Power Saving in 802.11

Due to limited energy reserves in mobile wireless devices, it is a desirable to dissipate as little power as possible for wireless communication activities. IEEE 802.11 provides methods to support power saving at the end stations. The power saving is achieved by switching between Active Mode (AM) and Power

Save (PS) mode.

When an MS does not have to be continuously working, it can switch to a sleep mode for a fraction of every superframe. The MS needs to wake up periodically to receive possible incoming data frames from the AP. The IEEE 802.11 protocol requires that the AP maintain a list of the MSs in PS mode. When a frame arrives at the AP and it needs to be forwarded to one of those MSs, the AP temporarily buffers that frame until the MS is Active Mode again.

However, no method to support power saving in the APs is supported by the IEEE 802.11 protocol set. Later, in section 3.4, a power saving access point architecture is explained which is used in this thesis in the design of solar-powered ESS mesh networks.

3.3 ESS Mesh Networking

APs are layer 2 internetworking devices. In contrast to Routers which work at the third layer, APs, similar to Bridges, use the MAC layer header in processing frames. In another words, APs acts as a bridge between the wireless and wired LANs. Three types of wireless networking architectures are supported by IEEE 802.11 standard: the Basic Service Set (BSS), the Independent Basic Service Set (IBSS), and the Extended Service Set (ESS).

BSS is the most common configuration where a single AP is connected to the wired network and acts as a gateway to the external network for the MSs associated with it. In this type of architecture all the traffic goes through the AP, and even the local traffic between MSs will be forwarded by the AP. The

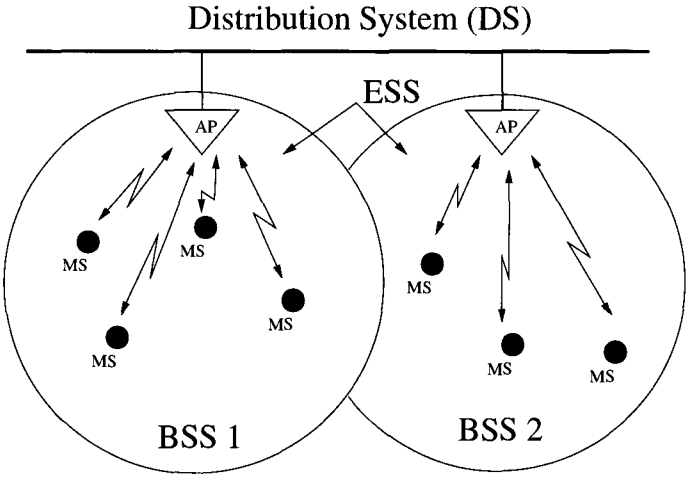

Figure 3.1: Example of BSS and ESS configurations

IBSS WLAN is formed by a number of MSs communicating in ad-hoc mode. In this mode, since no AP is available to forward frames, MSs forward frames for each other.

When several BSSs are interconnected at layer two, the whole set is called an ESS. The Distribution System (DS) which interconnects the APs uses the four-address scheme defined under IEEE 802.11 for exchanging frames between APs. If wireless links are used in the distribution system, it is called a Wireless Distribution System (WDS). An example of BSS and ESS configurations is shown in Figure 3.1.

One type of ESS network is an ESS mesh network. These networks are currently being standardized under IEEE 802.11s ESS mesh [15], which intends to promote interoperability between different vendor solutions. ESS mesh networks provide IEEE 802.11 coverage for mobile stations (MSs) and also per-

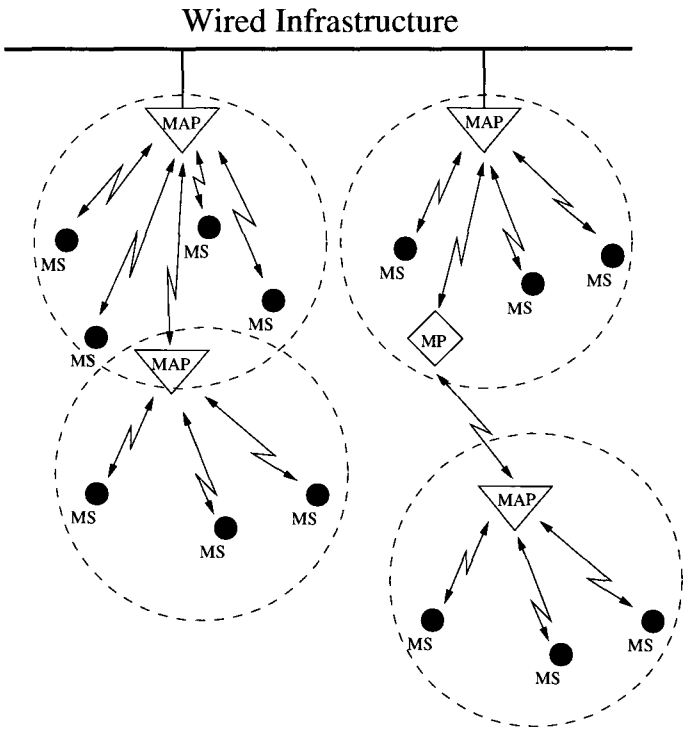

Figure 3.2: Example of an ESS Mesh Network

form wireless distribution (WDS) using multihop relaying between mesh APs (MAPs) and mesh points (MPs). A mesh point is a relay node that does not provide coverage for end user stations [15]. Figure 3.2 shows a sample ESS mesh network.

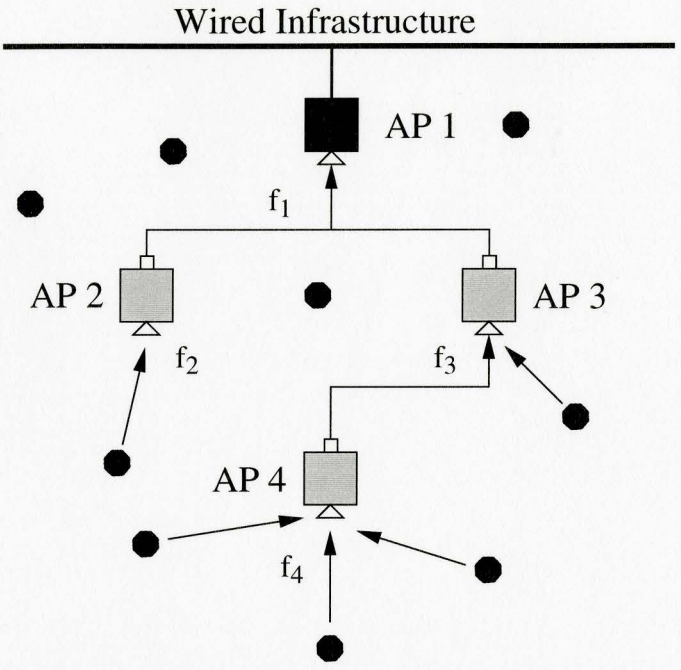

Figure 3.3: Solar Powered ESS Mesh Architecture

3.4 Power Saving ESS Mesh Infrastructure

In Figure 3.3 we show an example of the type of architecture under consideration. We adopt the convention that a radio which is used for MS coverage is denoted by a small triangle, and a radio which is dedicated to backhaul relaying is represented by a small box. In Figure 3.3 AP 1 is a node that is connected to the wired infrastructure. The other APs are solar/battery powered and in this example each contain two radio interfaces. APs 2 and 3 use their relay radio to backhaul traffic through AP 1's coverage radio on frequency f_1. Similarly, AP 4 relays traffic through AP 3 on f_3.

To reduce power consumption in solar powered APs, the nodes should spend as much time as possible in a low power conserving sleep state. Under normal conditions this power saving should not violate the QoS needed to support the traffic being carried. In [21] a power saving ESS mesh architecture is proposed based on extensions to IEEE 802.11e [16]. In this protocol a power saving AP includes a network allocation map (NAM) in its beacon broadcasts which specifies periods of time within the superframe when it is unavailable. It is during these periods that the AP may assume an inactive state and conserve power.

An example of this is shown in Figure 3.4. In the figure activity for a single inter-beacon period is given. The upper time line shows channel activity and the lower one shows the NAMs that are signaled by the AP beacons. In this example two HCCA (or EDCA) periods (each lasting 30 ms) have been scheduled and the AP advertises the NAMs as shown so that power saving can occur when the channel is not needed. In this case the AP is satisfying the transmission requirements of the mobile stations, and using the remaining time for AP power saving. An algorithm for dynamically updating the NAMs was proposed in [21].

The AP can also choose to *force* a level of power saving activity *regardless* of mobile station transmission requirements. This is referred to as forced power saving (FPS). An example of this is shown in Figure 3.5 where the AP advertises a NAM that restricts the activity of the AP to a maximum of 50% of the inter-beacon interval. If we define T_f to be the total forced power saving time per

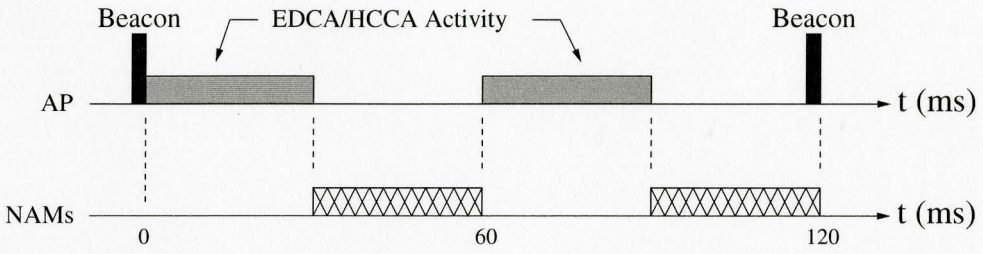

Figure 3.4: Power Saving AP Example with 2 HCCA/EDCA Service Periods.

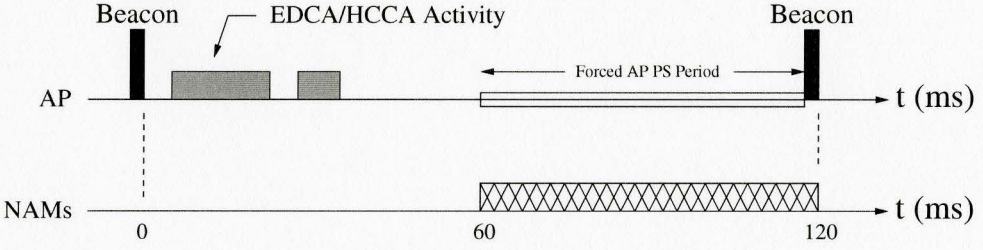

Figure 3.5: Forced AP Power Saving (FPS) with 50% Offered Capacity.

inter-beacon period, t_B, then the normalized offered capacity is defined by

$$OC = 1 - \frac{T_f}{t_B}. \tag{3.1}$$

OC is simply the fraction of the timeline that the AP is making available to support data traffic. Note that in addition to the forced power saving interval(s) there may also be power saving periods whose duration is updated dynamically according to MS packet backlogs. For this reason, T_f is the *minimum* level of power saving that will be achieved by the AP. FPS is a very important feature which allows the AP to place a strict upper bound on the energy expended per beacon interval. This capability is used in the outage control algorithm proposed in Section 5.2.

Chapter 4

Solar Powered PSAP Design

4.1 Overview

In the design of a Solar Powered Mesh AP (SMAP), the cost of the solar panel and battery can be a significant fraction of the total. For this reason the resource allocation must be done accurately to avoid under/over estimation in the amount of resources required to achieve a certain level of network performance and reliability.

In a SMAP, the energy is generated in the solar panel and it is consumed by the AP board and its wireless network interface. Also, a battery is needed to make the continuous operation of the system possible during the night when there is no solar radiation. Based on the energy conservation law, the energy flow model for the above components inside a SMAP can be formulated.

Both the solar radiation energy and the traffic load in a mesh network

have a stochastic nature. This results in uncertainties that must be considered in the design and performance evaluation of SMAPs. The performance of a Solar-Powered Mesh AP (SMAP) is measured in the term of the system outage probability (P_{out}), where outage means forced shut-down of the SMAP due to the lack of power. In the literature, this outage event is normally referred to as a node death event.

One complexity in the design of SMAPs is to determine the AP loading. If one was to know in advance the future arrival process of load impinging on the AP, then solar panel/battery provisioning would be relatively straightforward. One could use this information in conjunction with the meteorological data to do a very good design. However, such detailed knowledge would never be available in practice. In this chapter, we propose a design methodology which helps us to estimate a design capacity profile based on the available information of the average required capacity. In the proposed design methodology, an averaged offered capacity profile for each network node is first defined. The capacity profile is a time function which represents the average workload for which the node in question is designed. For a given geographic location, public meteorological data can then we used to configure the node subject to a target outage probability.

In the rest of this chapter, first the structure for a typical SMAP is introduced and the energy flow model is presented. Then, contour plots for two different cities are compared. Also the effect of AP power consumption on the system size is discussed. Finally, the proposed design methodology is explained.

4.2 Solar Powered AP Design and Energy Flow Model

Figure 4.1 shows a simplified block diagram of a solar powered ESS mesh node. The solar panel and battery are connected to the AP through a charge controller which performs functions such as battery over-/under-charge protection. In the energy flow model, we define $\mathcal{E}_{panel}(k)$ to be the energy produced in the solar panel over the time increment $[(k-1)\Delta, k\Delta]$, where Δ is the time-step length considered. In PV systems designed using publicly available meteorological data, data collection and modelling is done in discrete time, and more than sufficient accuracy is obtained using 1 hour Δ increments. The solar panel size is given by S_{panel}, and is usually rated in watts at peak solar insolation. We also define $\mathcal{B}(k)$ to be the residual battery energy stored at time $k\Delta$, and $\mathbf{B}_{max}$ is defined to be the total battery capacity. If we assume that $\mathcal{L}(k)$ is the load energy demand over the time duration $[(k-1)\Delta, k\Delta]$, then we can write that [39],

$$\begin{aligned} \mathcal{B}(k) &= \min\{\max[\mathcal{B}(k-1) + \mathcal{E}_{panel}(k) \\ &\quad -\mathcal{L}(k), \mathbf{B}_{outage}], \mathbf{B}_{max}\}. \end{aligned} \tag{4.1}$$

$\mathbf{B}_{outage}$ is the maximum allowed depth of discharge, based on safety and battery life considerations [30]. When $\mathcal{B}(k) < \mathbf{B}_{outage}$, the charge controller will disconnect the MAP/MP load and the node will experience a radio outage.

Using public solar insolation data for a particular geographic location [32] [31] and the energy flow model, a worst-case design can be performed.

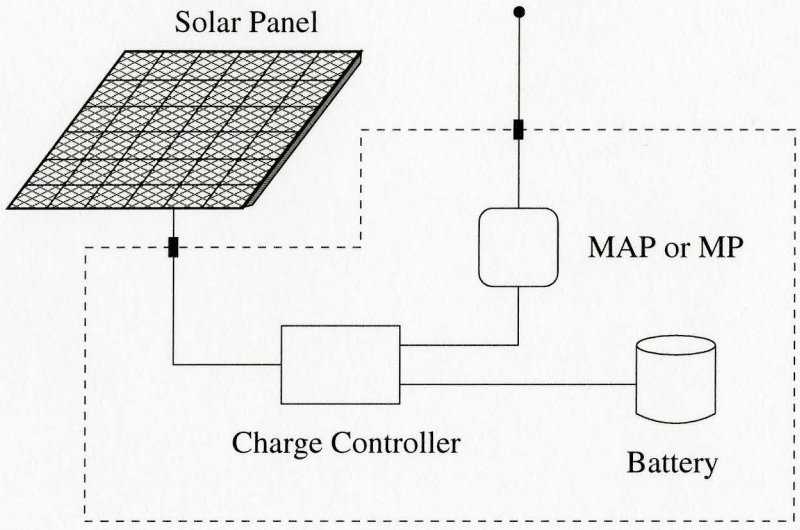

Figure 4.1: Basic SMAP Components

This is done by assuming that $\mathcal{L}(k) = \mathbf{P}_{APmax}\Delta$ for all k, where $\mathbf{P}_{APmax}$ is the peak power consumption of the AP. Using Equation 4.1 a discrete-time simulation of the node can be done over the solar insolation history of the desired location. Using this method it is straightforward to produce a set of solar panel versus battery capacity contours of constant outage probability.

An example is shown in Figure 4.2 assuming a constant single-radio AP power consumption of 2.5W, which is typical for commercial APs. The graphs show plots of solar panel size versus battery capacity for curves of constant outage probability. Comparing the two geographic locations, the differences in node configuration are very large. In the more temperate case (Toronto), provisioning a solar node for negligible outage (i.e., $< 10^{-4}$) requires about a 60W solar panel, which alone would be a significant fraction of the total node

cost. In the Phoenix case the same performance can be obtained with a 20-25W panel.

It is important to note that with 1-hour meteorological data, accurate estimates of outage probability contours below about 10^{-4} is very difficult, since available data only spans several decades. In any case the proposed outage control algorithm in Section 5.2 can be used to reduce outage even if the designs have been done using higher outage probability targets.

For each outage probability in Figure 4.2, there are a continuum of feasible battery/panel combinations. In this thesis we assume that this selection is done on the basis of minimum cost. Using the linear relationship between cost and both panel and battery size (which is usually the case), lines of constant cost and slope can be superimposed on Figure 4.2. The optimum panel and battery to choose corresponds to the line that intersects the desired outage curve tangentially.

In Figure 4.3 another example is shown for different values of fixed AP power consumption using data for Toronto and a 10^{-3} outage probability. It can be seen that the resources required are very sensitive to AP power consumption. Reducing the power consumption of the AP from 2.5W to 1.25W, for example, drops the required panel *and* battery size each by about 50%. For this reason, low AP power consumption is very desirable. Although it is possible to reduce AP power consumption using judicious design and component selection, obtaining a single-radio power consumption below about 1W is currently very difficult. This situation is exacerbated by the fact that ESS mesh nodes are increasingly deployed with multiple radio interfaces. This pushes the

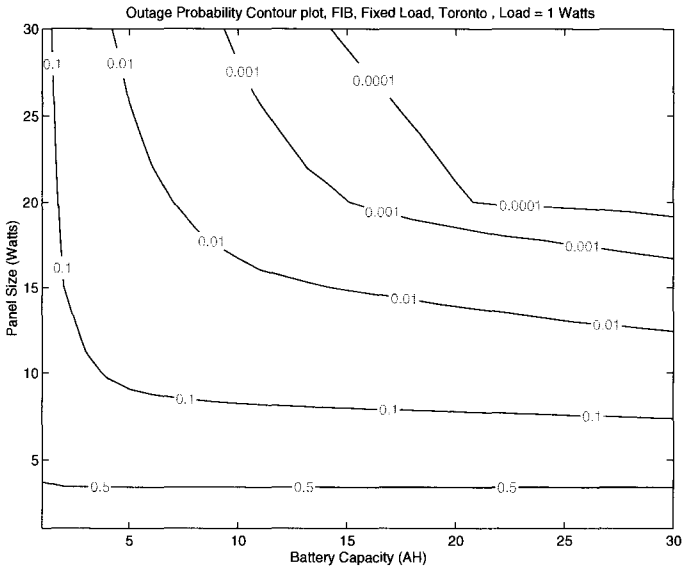

(a) Toronto, CAN.

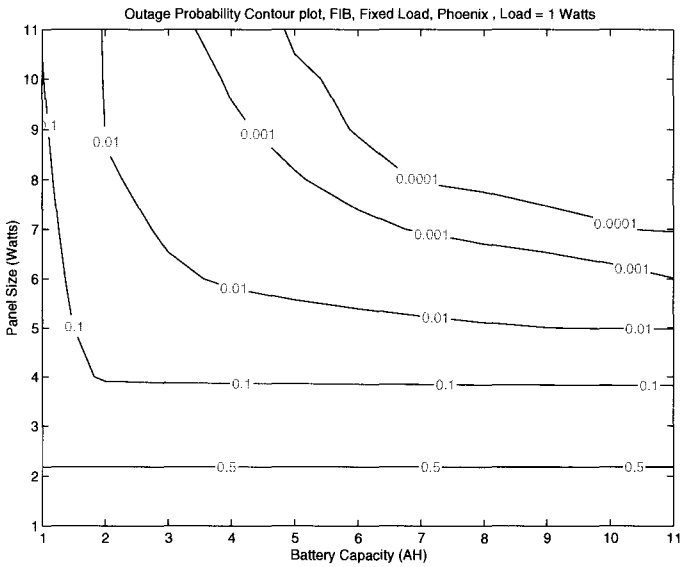

(b) Phoenix, Az.

Figure 4.2: Outage Example for Toronto and Phoenix, 1W AP Loading

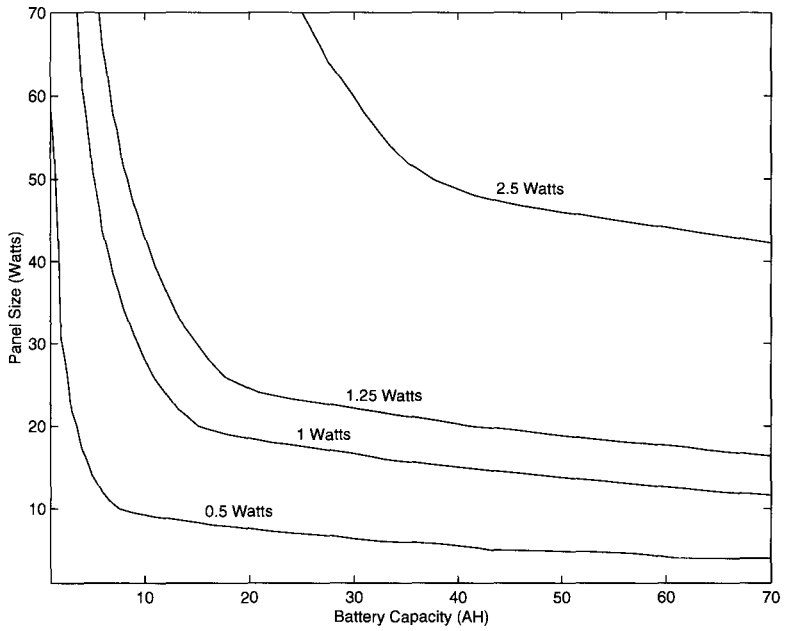

Figure 4.3: Comparison of Fixed-outage Curves for Different AP Power Consumption, when $P_{out} = 10^{-3}$

minimum AP power consumption much higher.

The above discussion assumes that the AP operates at its maximum power consumption at all times, which is always the case in conventional APs. However, in many applications the utilization of the AP may be far below 100%, and a node configured using the above procedures may be greatly over-provisioned. This is especially true for outdoor deployments. In most outdoor cases, AP utilization is expected to be very low during evening and nighttime hours, and power-aware AP protocols could translate this low utilization into reductions in panel/battery size. In temperate regions, AP utilization is also expected to

exhibit strong yearly cycles which further reduce utilization during the times of the year when solar insolation is at a minimum. This is significant since these are the times which dictate the panel and battery sizes. In the following section we introduce a statistical solar powered node provisioning methodology using the power saving AP protocol explained in section 3.4.

4.3 Statistical Provisioning Using Offered Capacity and Energy Profiles

Statistical provisioning is complicated by the fact that future loading conditions are not known exactly. However, this is strongly compensated for by the fact that the solar panel and battery averages solar energy input and power dissipation over long time periods. For this reason reasonable photovoltaic system designs can often be done based on averaged workloads.

The statistical design methodology starts with an Averaged Offered Capacity Profile, AOCP. $\texttt{AOCP}(\cdot)$ is defined to be a time function which spans a single year, i.e., $\texttt{AOCP}(k)$ is defined to be the ensemble average over all years of the offered capacity that the system is designed for, over the interval of time $[(k-1)\Delta, k\Delta]$. In practice there will be uncertainty as to how to predict $\texttt{AOCP}(\cdot)$, and in some cases worst-case values may be chosen. As in other capacity deployment situations, designers will often have a good idea of a reasonable profile through experience with similar deployments. It is important to note that the particular value of $\texttt{AOCP}(k)$ does not mean that this is the peak

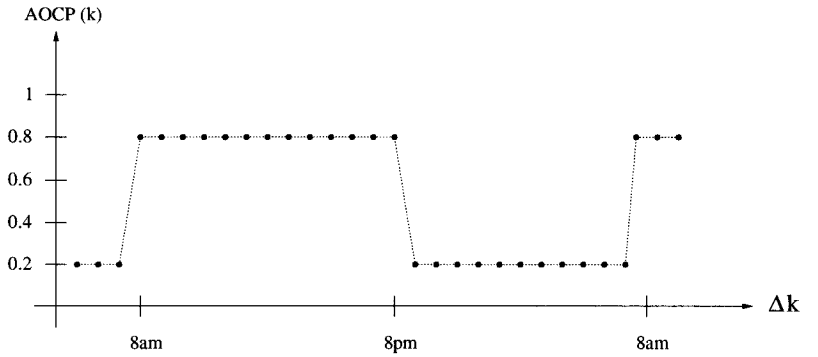

Figure 4.4: Example Daily AOCP for an Outdoor AP

capacity that is offered to users of the AP throughout $[(k-1)\Delta, k\Delta]$. The dynamic power saving protocol will permit full utilization of the AP when it is needed. Rather, AOCP(k) specifies an ensemble *average* of the AP activity level over that period.

An example of an AOCP over a single day for an outdoor coverage area is shown in Figure 4.4. The profile is normalized so that a value of 1 corresponds to full utilization (and power consumption) of the AP. In this example the averaged offered AP capacity during daytime hours (8am to 8pm) is 0.8. The AOCP drops to 0.2 during nighttime hours when mobile users are not expected to be present in this outdoor coverage area. In the example shown we assume that this daily profile would be repeated to generate the complete yearly AOCP. However, in temperate climates average outdoor winter traffic loading may be much lower than in the summer months, and thus a more accurate offered capacity profile may be used.

Once AOCP($\cdot$) has been determined it is used to compute a Yearly Energy

Profile, $\texttt{YEP}(\cdot)$ for the AP, i.e.,

$$\texttt{YEP}(k) = \mathcal{F}[\texttt{AOCP}(\cdot)], \tag{4.2}$$

for all k. The function $\mathcal{F}[\cdot]$ translates the average activity of the AP into an average energy consumption over $[(k-1)\Delta, k\Delta]$. This translation is generally straightforward given knowledge of the AP design, and of the type of traffic that the AP is expected to carry. It also requires some assumptions regarding the fraction of time that the AP is listening, receiving and transmitting. In the results in this thesis we assume the worst-case power consumption mode for the AP when it is active. Any fixed radio-independent power consumption components of the AP must also obviously be included. Sufficient accuracy can be obtained by considering each interval independently, i.e., $\texttt{YEP}(k) = \mathcal{F}[\texttt{AOCP}(k)]$. In order to determine the required system configuration, meteorological data is used in conjunction with the energy profile to size the battery and solar panel combination as previously discussed in Section 4.2.

Chapter 5

Outage Control and Capacity Deficit

5.1 Overview

Full depletion of the battery charge, called outage, is a very undesirable event. When the system is in the outage state the battery is totaly empty and no network traffic can be supported even if it is an emergency or a high-priority. In addition, in that state the board is no longer functioning, and the system is inaccessible even for administrative purposes.

One possibility for the SMAP controlling system to avoid an outage event is to use FPS mode explained in section 3.4 to artificially reduce the offered capacity. This may result in capacity deficit. Capacity deficit occurs when the

required capacity exceeds the capacity that is offered by the SMAP. In many situations, it may be acceptable to try to avoid an outage event at the cost of having some capacity deficit. This is similar to channel reservation in hand-off QoS provisioning, where it is considered acceptable to drop an incoming call to be able to support a potential ongoing hand-off call in the future.

In the previous chapter, a design methodology was introduced which can size the access point subject to a workload function defined by the average offered capacity profile. However, the proposed design methodology is statistical since future load conditions and solar insolation may not exactly match that for which the node was designed. Therefore, even when the system is designed for a very small outage probability there is still a chance of poor performance. For example, an excessive capacity demand over a period of time or a long and unexpected string of gloomy days may easily result in an outage event.

The above issues mandate the use of an adaptive control scheme to handle the uncertainties by trading off capacity deficit for outage probability. However, both the required capacity in a mesh network and the incoming solar radiation energy have a stochastic nature which makes the problem fairly complicated. As we will see later, an efficient solution to this problem involves making an optimal decision for a stochastic control problem.

In this chapter some control algorithms are proposed for improving the performance of the SMAP. First, the objective behind applying traffic control algorithms is explained and then the problem of efficient control is formulated as a stochastic control problem. After that, two heuristic control schemes are proposed.

5.2 Outage Control and Capacity Deficit Algorithms

When traffic is consistent with the offered capacity profile then the outage performance of the node will conform to that associated with the solar insolation data used in the design. Every effort should be made to ensure that the profile is such that it accommodates future loading conditions. Unfortunately, this will not always be the case, and average loading may exceed the AP's design characteristics. When this happens the AP may experience outages that are more frequent than that for which the AP was provisioned. In addition, there is no guarantee that future solar irradiation will be consistent with the past data used for the design. Both these random effects may lead to outage rates that are higher than the design target.

Normally IEEE 802.11 APs will be provisioned for a negligible outage rate. This may be considered a strong practical requirement, and is to ensure that communications for emergency, maintenance, and other high priority traffic can always be carried by the network. In addition to this requirement, we assume that the normalized level of AP activity should never drop below some value, $\mathbf{U}_{min}$, such as 20%, otherwise the operation of the AP would be too impaired. In the next section, control algorithms are introduced whose intent is to sometimes artificially reduce the capacity offered by the AP. The proposed adaptive control schemes intelligently adjust the amount of the capacity offered during each time-step. The objective is to maximize system reliability for a given system configuration, while trying to keep the capacity deficit as low as

possible.

The problem of efficient control can be formulated as a stochastic control problem. As before $\mathcal{L}(k)$ is defined to be the energy loading of the AP during the time interval $[(k-1)\Delta, k\Delta]$. This is the energy that would be required for the AP to successfully carry the offered traffic during this time interval. We then define the *actual* energy loading on the AP during $[(k-1)\Delta, k\Delta]$ to be $\mathcal{E}_a(k)$. In the absence of any control, $\mathcal{E}_a(k) = \mathcal{L}(k)$, but when a control mechanism is in place, the activity level of the AP may sometimes be artificially reduced to save power, i.e.,

$$\mathcal{E}_a(k) = \min(\mathcal{L}(k), \mathcal{E}_{max}(k)), \tag{5.1}$$

where $\mathcal{E}_{max}(k)$ is a control variable that specifies the maximum energy consumption in the next interval. The actions of the control variable lead to an energy deficit, $\mathcal{E}_{def}(k)$, defined by

$$\mathcal{E}_{def}(k) = \mathcal{L}(k) - \mathcal{E}_a(k). \tag{5.2}$$

$\mathcal{E}_a(k)$ is not permitted to drop below the value needed to provide $\mathbf{U}_{min}$ AP activity level, i.e., $\mathcal{E}_a(k) \geq \mathcal{F}(\mathbf{U}_{min})$. The objective of the control scheme is to satisfy the target outage rate while reducing the capacity deficit as much as possible. For a given loading condition, the optimum control scheme is to select $\mathcal{E}_a(k)$ for all k, such that the energy deficit over all time is minimized, i.e.,

$$\min_{\{\mathcal{E}_{max}(k)\}} \sum_{k=0}^{\infty} \mathcal{E}_{def}(k), \tag{5.3}$$

subject to

$$\mathcal{B}(k) = \min\{\max[\mathcal{B}(k-1) + \mathcal{E}_{panel}(k) - \mathcal{E}_a(k), \mathbf{B}_{outage}], \mathbf{B}_{max}\} \tag{5.4}$$

$$Pr\{\bigcap_k (\mathcal{B}(k) > \mathbf{B}_{outage})\} \geq 1 - \mathbf{P}_{outage} \tag{5.5}$$

$$\mathcal{E}_a(k) \geq \mathcal{F}(\mathbf{U}_{min}). \tag{5.6}$$

Equation 5.4 is the modified energy flow equation for the system, Equation 5.5 is our outage requirement, and Equation 5.6 is the constraint on minimum AP activity. Normally the AP will be designed to a zero outage probability target and in this case Equation 5.5 is equivalent to the requirement that $\mathcal{B}(k) > \mathbf{B}_{outage}$ for all k. Unfortunately Equation 5.3 is an extraordinarily hard optimization. In the next section we consider a simple mechanism based on a classical control theory approach.

5.3 On/Off and Proportional Capacity Deficit Control

When the battery energy is low, the frequency of outage can be reduced by decreasing the capacity offered by the AP, i.e., by increasing the capacity deficit. The proposed algorithm consists of two related components. The first is a classic On/Off controller which restricts the activity of the AP to $\mathbf{U}_{min}$ when the battery state of charge crosses a threshold, denoted by $\mathbf{L}_{th}$. In order to implement this scheme we define $\mathbf{P}_{Umin}$ to be the worst-case power consumption of

the AP when operating at $\mathbf{U}_{min}$. The basic on/off controller sets the maximum energy that will be dissipated in the next time step, $\mathcal{E}_{max}(k)$, as follows,

$$\mathcal{E}_{max}(k) = \begin{cases} \mathbf{P}_{APmax}\Delta, & \mathcal{B}(k-1) \geq \mathbf{L}_{th} \\ \mathbf{P}_{Umin}\Delta, & \mathcal{B}(k-1) < \mathbf{L}_{th}. \end{cases} \tag{5.7}$$

In Equation 5.7, the term $\mathbf{P}_{APmax}\Delta$ represents the peak energy that the AP can dissipate over Δ, and thus when the battery state of charge is above $\mathbf{L}_{th}$, the controller does not restrict the operation of the AP. However, when the battery energy is below $\mathbf{L}_{th}$, the activity level of the AP is restricted to be below $\mathbf{P}_{Umin}\Delta$.

The actions of the controller are specified in terms of AP energy usage constraints. In practice this must be translated into radio/node activities. A simple way to do this is to assume the worst-case power consumption of the AP, $\mathbf{P}_{APmax}$, and translate that into a maximum activity level per superframe. Assuming that the quiescent power consumption of the AP is $\mathbf{P}_{APmin}$, then it can easily be shown that the maximum fraction of time that the AP can be active during interval k is given by

$$OC(k) = \frac{\mathcal{E}_{max}(k) - \Delta\mathbf{P}_{APmin}}{\Delta(\mathbf{P}_{APmax} - \mathbf{P}_{APmin})}. \tag{5.8}$$

This expression is the normalized offered capacity discussed in Section 3.4, and Equation 3.1 can be used with this result to set the forced power saving (FPS) boundaries needed when the control algorithm is active.

A disadvantage of On/Off control alone is that the transition into active control occurs very abruptly. In our case this means that the AP could be offering full capacity at one instant, then $\mathbf{U}_{min}$ capacity at the next, and vice

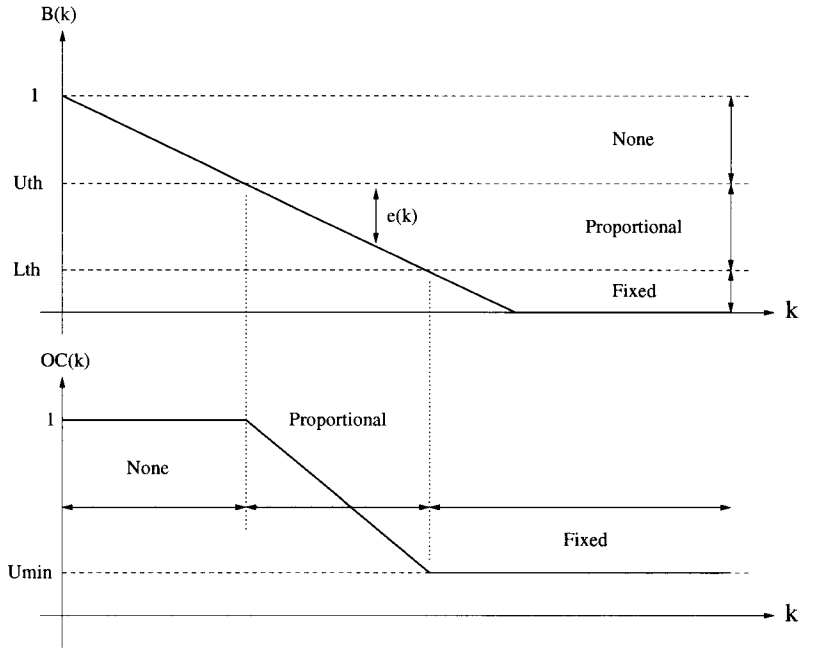

Figure 5.1: Control Algorithm Operation

versa. A much more desirable behavior would be to more gracefully add energy deficit as the battery energy reserves decrease. This is the objective of the proportional control algorithm. We define the error signal as $e(k) = \mathbf{U}_{th} - \mathcal{B}(k-1)$, where $\mathbf{U}_{th}$ is the threshold above which no control is exercised. When the controller is active, the maximum energy available for the next time step, $\mathcal{E}_{max}(k)$, is given by $\mathbf{P}_{APmax}\Delta - Ke(k)$. The constant K controls how aggressively we add energy deficit as our state of charge drops. In our case we select K such that the energy expended is $\mathbf{P}_{Umin}\Delta$ when $\mathcal{B}(k-1)$ reaches $\mathbf{L}_{th}$. At that point the on/off control is activated. This provides a piece-wise continuous transition between the two algorithms. Using this simple criterion we find that

$K = \Delta(\mathbf{P}_{APmax} - \mathbf{P}_{Umin})/(\mathbf{U}_{th} - \mathbf{L}_{th})$. The complete control algorithm is as follows.

$$\mathcal{E}_{max}(k) = \begin{cases} \mathbf{P}_{APmax}\Delta & \mathcal{B}(k-1) > \mathbf{U}_{th} \\ \mathbf{P}_{Umin}\Delta & \mathcal{B}(k-1) < \mathbf{L}_{th} \\ \mathbf{P}_{APmax}\Delta - K(\mathbf{U}_{th} - \mathcal{B}(k-1)) & \text{otherwise} \end{cases}$$

Figure 5.1 shows an example of how the control algorithm operates. The upper figure shows $\mathcal{B}(k-1)$ ramping down from full battery charge to zero. The lower figure shows the corresponding offered capacity, $OC(k)$. Provided the battery charge is above $\mathbf{U}_{th}$, no control at all is exercised and all the AP capacity is available for carrying traffic. In the region between $\mathbf{U}_{th}$ and $\mathbf{L}_{th}$ the offered capacity decreases in proportion to the size of the error signal, $e(k)$. Finally, when $\mathcal{B}(k-1)$ is below $\mathbf{L}_{th}$ a fixed capacity sufficient for supporting $\mathbf{U}_{min}$ is offered. In the performance chapter we will consider both algorithms discussed above, i.e., On/Off and Proportional On/Off control.

5.3.1 Selection of $\mathbf{L}_{th}$

In the above controllers, the selection of $\mathbf{L}_{th}$ is very important. In the proposed algorithm $\mathbf{L}_{th}$ is selected when the AP is configured using the meteorological data for that location. According to Equation 5.7, the peak power consumption of the AP is upper bounded by $\mathbf{P}_{Umin}$ when on/off control is active. When this is happening we can model the system as an AP whose AOCP is constant and offering a capacity needed for $\mathbf{U}_{min}$, i.e., $\texttt{AOCP}(k) = \mathbf{U}_{min}$ for all k. Using this offered capacity profile, the designed system is simulated with the meteo-

rological data as in Section 4.2. As the simulation is run the minimum value for battery state of charge is recorded. One minus this minimum value is then used as the threshold, $\mathbf{L}_{th}$.

5.4 Lower Bound for Capacity Deficit

The purpose of the control algorithms is to avoid outage events and to guarantee a minimum activity level of $\mathbf{U}_{min}$. As explained in the previous sections, the control algorithms reduce the offered capacity to reserve energy for the future. In another words, the control algorithms move the energy forward in time by withholding it. The resulting capacity deficit can be measured to compare the performance of different control schemes.

In this section we prove that there exists a lower bound for this capacity deficit. This bound would be the capacity deficit performance that can be achieved by the optimal control scheme. In what follows we will show that for the case where no control scheme is used if we reinterpret the outage points as having points with zero offered capacity or full capacity deficit, then it yields the lowest possible capacity deficit. Let us call this scheme as the no-control scheme and we will use "nc" as the subscript for it. Also, we use "arb" subscript to refer to a scheme which can be any arbitrary control scheme. Now, we start the proof by a lemma.

Lemma 1. *If the initial battery charge for both the no-control and an arbitrary*

control scheme are equal, then for every k we have that

$$\mathcal{B}_{nc}(k) \leq \mathcal{B}_{arb}(k). \tag{5.9}$$

Proof. Without loss of generality we assume that $\mathbf{B}_{outage} = 0$. We prove this lemma by induction on k. For $k = 0$ it is trivial since we assume that the initial charges are equal. We now assume that Equation 5.9 holds for $k-1$ and we prove that it is true for k. Clearly, $\mathcal{E}_{panel}(k)$ and $\mathcal{L}(k)$ are equal for both schemes.

For the no-control scheme $\mathcal{E}_{max}(k)$ is always equal to $\Delta\mathbf{P}_{APmax}$, which means that it always tries to offer a normalized capacity, $OC(k)$, of 1. Using Equation 5.1, for the arbitrary scheme we always have $\mathcal{E}_a^{arb}(k) \leq \mathcal{L}(k)$. The energy flow model in Equation 4.1 can be used to write $\mathcal{B}(k)$ given $\mathcal{B}(k-1)$. Assuming that the lemma is true for $\mathcal{B}(k-1)$, we can write that

$$\mathcal{B}_{nc}(k-1) + \mathcal{E}_{panel}(k) \leq \mathcal{B}_{arb}(k-1) + \mathcal{E}_{panel}(k). \tag{5.10}$$

If the battery state of charge, $\mathcal{B}_{nc}(k-1)$, is higher than $\Delta\mathbf{P}_{APmax}$ then it is guaranteed that the no-control scheme will be able to fully supply the load during the next time slot and we have that $\mathcal{E}_a^{nc}(k) = \mathcal{L}(k)$. Therefore,

$$\mathcal{E}_a^{arb}(k) \leq \mathcal{E}_a^{nc}(k) \quad if\ \mathcal{B}_{nc}(k-1) \geq \Delta\mathbf{P}_{APmax}. \tag{5.11}$$

If we multiply Equation 5.11 by -1 and add it to Equation 5.10 we obtain

$$\mathcal{B}_{nc}(k-1) + \mathcal{E}_{panel}(k) - \mathcal{E}_a^{nc}(k) \leq \mathcal{B}_{arb}(k-1) + \mathcal{E}_{panel}(k) - \mathcal{E}_a^{arb}(k). \quad (5.12)$$

Since the *Max* and *Min* operations do not change the direction of the inequality we can write that

$$\begin{aligned} &\min\{\max[\mathcal{B}_{nc}(k-1) + \mathcal{E}_{panel}(k) - \mathcal{E}_a^{nc}(k), 0], \mathbf{B}_{max}\} \leq \\ &\min\{\max[\mathcal{B}_{arb}(k-1) + \mathcal{E}_{panel}(k) - \mathcal{E}_a^{arb}(k), 0], \mathbf{B}_{max}\}, \end{aligned} \quad (5.13)$$

which is equivalent to

$$\mathcal{B}_{nc}(k) \leq \mathcal{B}_{arb}(k). \quad (5.14)$$

However, if $\mathcal{B}_{nc}(k-1) < \Delta\mathbf{P}_{APmax}$, depending on $\mathcal{L}(k)$ and $\mathcal{E}_{panel}(k)$ the system may not be able to support $\mathcal{L}(k)$ entirely. In that case we have

$$\mathcal{E}_a^{nc}(k) = \min[\mathcal{L}(k), \mathcal{B}_{nc}(k-1) + \mathcal{E}_{panel}(k)], \quad (5.15)$$

and for $\mathcal{B}_{nc}(k)$ we can write,

$$\mathcal{B}_{nc}(k) = \max[\mathcal{B}_{nc}(k-1) + \mathcal{E}_{panel}(k) - \mathcal{E}_a^{nc}(k), 0]. \quad (5.16)$$

If we substitute Equation 5.15 into Equation 5.16 we obtain

$$\begin{aligned} \mathcal{B}_{nc}(k) &= \max[\mathcal{B}_{nc}(k-1) + \mathcal{E}_{panel}(k) \\ &- \min\{\mathcal{L}(k), \mathcal{B}_{nc}(k-1) + \mathcal{E}_{panel}(k)\}, 0], \end{aligned} \quad (5.17)$$

therefore for $\mathcal{B}_{nc}(k)$ we can write that

$$\mathcal{B}_{nc}(k) = \begin{cases} \mathcal{B}_{nc}(k-1) + \mathcal{E}_{panel}(k) - \mathcal{L}(k) & \mathcal{L}(k) < \mathcal{B}_{nc}(k-1) + \mathcal{E}_{panel}(k) \\ 0 & \text{otherwise,} \end{cases}$$

and for $\mathcal{B}_{arb}(k)$ we have

$$\mathcal{B}_{arb}(k) = \min\{\max[\mathcal{B}_{arb}(k-1) + \mathcal{E}_{panel}(k) - \mathcal{E}_a^{arb}(k), 0], \mathbf{B}_{max}\}. \tag{5.18}$$

There are two cases, i.e., if $\mathcal{L}(k) \geq \mathcal{B}_{nc}(k-1) + \mathcal{E}_{panel}(k)$ then $\mathcal{B}_{nc}(k) = 0$ and clearly we have $\mathcal{B}_{nc}(k) \leq \mathcal{B}_{arb}(k)$. Otherwise, if $\mathcal{L}(k) < \mathcal{B}_{nc}(k-1) + \mathcal{E}_{panel}(k)$ then $\mathcal{B}_{nc}(k) = \mathcal{B}_{nc}(k-1) + \mathcal{E}_{panel}(k) - \mathcal{L}(k)$. However, we know that $\mathcal{E}_a^{arb}(k) \leq \mathcal{L}(k)$ and $\mathcal{B}_{nc}(k-1) \leq \mathcal{B}_{arb}(k-1)$ which lets us write that

$$\mathcal{B}_{nc}(k-1) + \mathcal{E}_{panel}(k) - \mathcal{L}(k) \leq \mathcal{B}_{arb}(k-1) + \mathcal{E}_{panel}(k) - \mathcal{E}_a^{arb}(k), \tag{5.19}$$

from which we can conclude that $\mathcal{B}_{nc}(k) \leq \mathcal{B}_{arb}(k)$. □

Theorem 1. *The no-control scheme yields the lowest capacity deficit of any control algorithm.*

Proof. We want to show that for the no-control scheme the capacity deficit is lower than that of any other arbitrary control scheme. We can write that

$$\mathcal{B}_{nc}(k) = \sum_{i=1}^{k} \mathcal{E}_{panel}(i) - \sum_{i=1}^{k} \mathcal{E}_a^{nc}(i) - \sum_{i=1}^{k} \mathcal{E}_{surplus}^{nc}(i) + \mathcal{B}_{initial}, \tag{5.20}$$

and

$$\mathcal{B}_{arb}(k) = \sum_{i=1}^{k} \mathcal{E}_{panel}(i) - \sum_{i=1}^{k} \mathcal{E}_{a}^{arb}(i) - \sum_{i=1}^{k} \mathcal{E}_{surplus}^{arb}(i) + \mathcal{B}_{initial}, \tag{5.21}$$

where $\mathcal{B}_{initial}$ is the initial battery charge and $\mathcal{E}_{surplus}(k)$ is the surplus energy not stored in the battery when it is full. For $\mathcal{E}_{surplus}(k)$ we can write that

$$\mathcal{E}_{surplus}(k) = \max[\mathcal{B}(k-1) + \mathcal{E}_{panel}(k) - \mathcal{E}_{a}(k) - \mathbf{B}_{max}\ , 0]. \tag{5.22}$$

Based on Lemma 1 and Equation 5.11 we can write that

$$\mathcal{E}_{surplus}^{nc}(k) \leq \mathcal{E}_{surplus}^{arb}(k), \tag{5.23}$$

which can be used to obtain

$$\sum_{i=1}^{k} \mathcal{E}_{surplus}^{nc}(i) \leq \sum_{i=1}^{k} \mathcal{E}_{surplus}^{arb}(i). \tag{5.24}$$

From Lemma 1 we have that $\mathcal{B}_{nc}(k) \leq \mathcal{B}_{arb}(k)$. If we substitute the terms with the right hand side of Equations 5.20 and 5.21, after some modification, we have that

$$\sum_{i=1}^{k} \mathcal{E}_{a}^{nc}(i) + \sum_{i=1}^{k} \mathcal{E}_{surplus}^{nc}(i) \geq \sum_{i=1}^{k} \mathcal{E}_{a}^{arb}(i) + \sum_{i=1}^{k} \mathcal{E}_{surplus}^{arb}(i). \tag{5.25}$$

This can be written as

$$\sum_{i=1}^{k} \mathcal{E}_{a}^{nc}(i) \geq \sum_{i=1}^{k} \mathcal{E}_{a}^{arb}(i) + \{\sum_{i=1}^{k} \mathcal{E}_{surplus}^{arb}(i) - \sum_{i=1}^{k} \mathcal{E}_{surplus}^{nc}(i)\}. \tag{5.26}$$

The value for the statement inside the braces is positive, therefore,

$$\sum_{i=1}^{k} \mathcal{E}_a^{nc}(i) \geq \sum_{i=1}^{k} \mathcal{E}_a^{arb}(i). \tag{5.27}$$

From Equation 5.2 we know that $\mathcal{E}_{def}(k) = \mathcal{L}(k) - \mathcal{E}_a(k)$. Also, we define the average capacity deficit to be

$$\overline{\mathcal{E}_{def}} = \lim_{j \to \infty} \frac{\sum_{i=1}^{j} \mathcal{E}_{def}(i)}{j}. \tag{5.28}$$

From Equation 5.27 we can write that

$$\sum_{i=1}^{k} \mathcal{L}(i) - \sum_{i=1}^{k} \mathcal{E}_a^{nc}(i) \leq \sum_{i=1}^{k} \mathcal{L}(i) - \sum_{i=1}^{k} \mathcal{E}_a^{arb}(i), \tag{5.29}$$

which can be written as

$$\sum_{i=1}^{k} \mathcal{E}_{def}^{nc}(i) \leq \sum_{i=1}^{k} \mathcal{E}_{def}^{arb}(i). \tag{5.30}$$

If we divide both sides by k and take the limit as $k \to \infty$, we obtain

$$\overline{\mathcal{E}_{def}^{nc}} \leq \overline{\mathcal{E}_{def}^{arb}}. \tag{5.31}$$

□

Based on Theorem 1, one simple way to estimate a lower bound for the capacity deficit is to perform the simulations without using any control algorithm, and then the amount of energy deficit is equal to the amount of energy needed to operate the system during the outage periods. This is true because we can reinterpret the outage points as points with full capacity deficit.

The exact amount of capacity deficit in a system is a function of the incoming load, and the incoming load is a random process. However, if we assume that the system is working at a fixed load, then for every simulation scenario we can determine the lowest possible capacity deficit needed to avoid outage events. In the next chapter we use the explained method to estimate a lower bound for the capacity deficit for fixed loads.

This lower bound can be used in comparing different control algorithms with the optimal behavior. If for some heuristic control algorithm the capacity deficit is close to this bound, we can conclude that the performance of the control algorithm is acceptable. In Section 6.3, we will use this method to compare the performance of the proposed control schemes with the optimal algorithm.

Chapter 6

Performance Results

6.1 Overview

In the previous chapters we proposed a design and resource allocation methodology for SMAPs. Also, control algorithms were introduced which can be used to improve the outage performance of a SMAP. In this chapter, we present results of simulation experiments conducted to evaluate the performance and effectiveness of the proposed methodology and control algorithms.

We use the proposed resource sizing method to determine the required configuration for solar-powered APs. The control schemes have also been investigated under variable and excess AP loading. In this chapter we will present some representative examples of our results. The solar panel was assumed to be fixed and tilted facing toward the equator, and the solar models used are briefly discussed in the chapter 2. In the experiments the meteorological data

for a location is partitioned into two, so that one can be used for the design, and the other can be used when simulating the system under test.

A non-ideal, temperature dependent battery model with an initial complete battery charge was assumed in the simulations [4, 40]. The chemical balance in a lead-acid battery is affected by the ambient temperature. As the temperature decreases, this balance changes such that less energy is available to the user at the battery terminals. For a typical lead-acid battery this reduction can be as much as 35% of battery capacity when the temperature reaches -20^oC. The nominal battery capacity is measured at a reference temperature. Battery vendors provide coefficient tables which can be used to determine the effective battery capacity at different temperatures as a fraction of the nominal capacity.

6.2 Single Node Design

When no power saving is done in the AP, its power consumption is relatively fixed. When the power saving algorithms explained in Section 3.4 are used, the power consumption of the AP is no longer fixed and it is dependent on the incoming load. In this case, the statistical provisioning method as explained in section 4.3 can be used to design the SMAP.

In this section we consider both of these cases. At first we do the design for a fixed AOCP which can be considered as the design methodology for a non-power saving AP. Then, variable load profiles and AOCP's are used in the sizing procedure. Finally, we compare the results.

In Figure 6.1 a plot of the various design options is shown using the AOCP

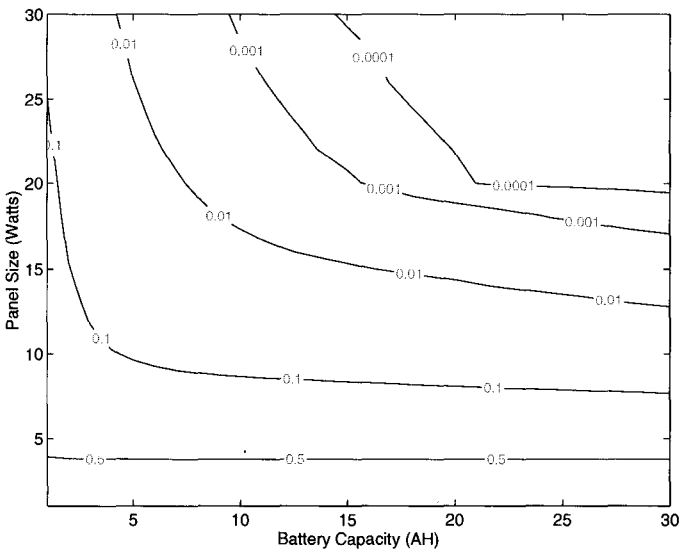

Figure 6.1: Contour Plot for an Example Outdoor AOCP1

from Figure 4.4. Let us denote this profile by AOCP1. We also consider another AOCP which is shown in Figure 6.3, denoted by AOCP2. The contour plot for AOCP2 is shown in Figure 6.2. AOCP2 corresponds to the case where the traffic load, in addition to day and night time variations, experiences seasonal changes. During the gloomy months the day time load drops to 20% and the night time load is only around 5%.

We have assumed that $\mathbf{P}_{APmax}$ is 2W for the node under consideration and that $\mathbf{P}_{APmin}$ is 20mW. Based on the generated contour plot, configuration sets corresponding to outage probabilities of 10^{-2}, 10^{-3} and 10^{-4} were determined. The optimum price panel and battery sizes for these outage probabilities are compared in the following table. A comparison between the non-power saving and power saving (AOCP1) designs shows that we are getting roughly a 2:1

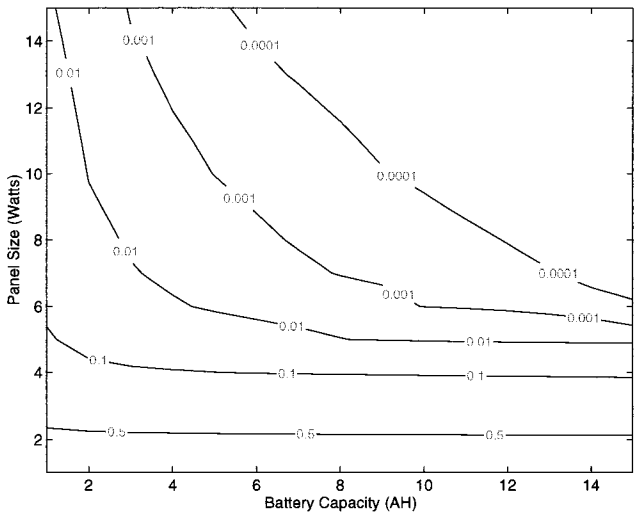

Figure 6.2: Contour Plot for an Example Outdoor AOCP2

improvement in both panel size and in battery size. Another comparison between the non-power saving and power saving (AOCP2) designs shows that the improvement can be as high as 4:1. This tradeoff would clearly not be possible for the existing IEEE 802.11 protocol, since the only option is to operate at full power consumption at all times.

Also, the results show that short-term fluctuations in the AOCP are not as important as long-term fluctuations. This means that when the AOCP has short-term fluctuations, the improvements achieved by the power saving techniques are to the level by which the average of the traffic load has changed. However, when the AOCP has long-term fluctuations the reduction in the system size are higher than the reduction for a system designed based on the average of the load profile. Therefore, in temperate climates yearly changes like seasonal variations

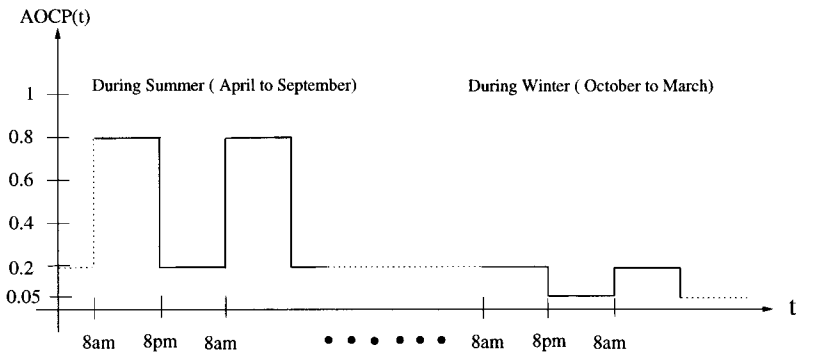

Figure 6.3: Example Daily AOCP2 for an Outdoor AP

in the traffic profile are of a higher importance than short-term variations.

6.3 Control Algorithms

The control schemes have been found to successfully prevent outage by selectively reducing the offered capacity. To perform experiments with significant potential for outage, we assume that the AP is exposed to excess loading, i.e., values much higher than that for which the AP was designed.

In Figures 6.4 and 6.5, results are given for an AP based on a $\mathbf{P}_{APmax}$ increased to 2W. Figure 6.4 shows the outage probabilities assuming a constant AOCP of 0.5. In these figures, the actual AP loading is the factor C_{Excess} times that for which the system was designed. When the on/off controller is active all measured outage probabilities were zero. It can be seen that when the controller is not active the outage probabilities rise sharply with excess load starting from values close to the original design outage targets. In these results

	No Power Saving		Power Saving AOCP1		Power Saving AOCP2	
$\mathbf{P}_{outage}$	$\mathbf{B}_{max}$	S_{pn}	$\mathbf{B}_{max}$	S_{pn}	$\mathbf{B}_{max}$	S_{pn}
10^{-2}	20.0	31.6	11.0	16.7	4.4	6.0
10^{-3}	30.1	38.0	15.7	20.0	7.8	7.0
10^{-4}	40.6	38.0	20.9	20.0	13.1	7.0

Table 6.1: Optimum Price Panel and Battery Configurations for different Load Profiles

$\mathbf{U}_{min}$ is assumed to be 10% and B_{th} is 0.1067 (or 11% of the battery capacity).

Figure 6.5 shows the price paid for eliminating outage in terms of capacity deficit. Three of the curves shown correspond to the case where the on/off control is active, and show that capacity deficit increases significantly with excess load. In the 10^{-4} outage design the capacity deficit reaches about 5% of the total capacity when operating with 200% excess loading. This value is a small fraction of the total capacity. Figure 6.6 shows the same graph when the proportional/on/off controller is used. It can be seen that the behavior is similar, but that the values of capacity deficit are higher overall than in the on/off case. This is to be expected since the proportional/on/off control is more aggressive at forcing power saving as the battery reserves decrease. However, it can still be seen that at 200% load, roughly the same value is achieved as in the on/off case for the 10^{-4} curve.

The results for the method explained in section 5.4 for estimating a lower

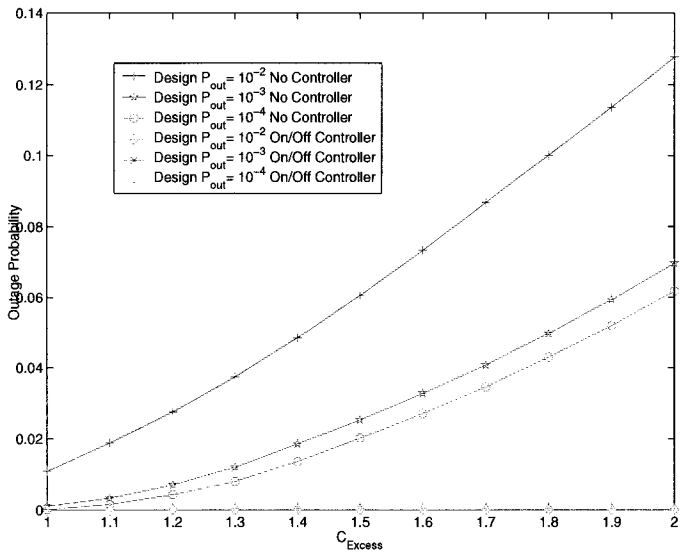

Figure 6.4: Outage Probability versus Excess Load

bound for the capacity deficit are shown in figures 6.5 and 6.6. It can be seen that for on/off controller the difference is negligible, specially when the load increases the performance of the on/off controller gets closer to the optimal performance. The results for the proportional/on/off controller show that although its performance is not better than on/off controller, it is acceptable and the difference in the

Figure 6.7 is from the same system and shows the effect of $\mathbf{U}_{min}$ on capacity deficit. As the minimum required capacity increases, the control algorithm reacts more aggressively, which results in higher capacity deficits. This is due to the fact that when $\mathbf{U}_{min}$ is higher, more power saving must be done in advance to ensure that the minimum capacity requirement can be guaranteed.

An advantage of the proportional/on/off controller is that it is less abrupt,

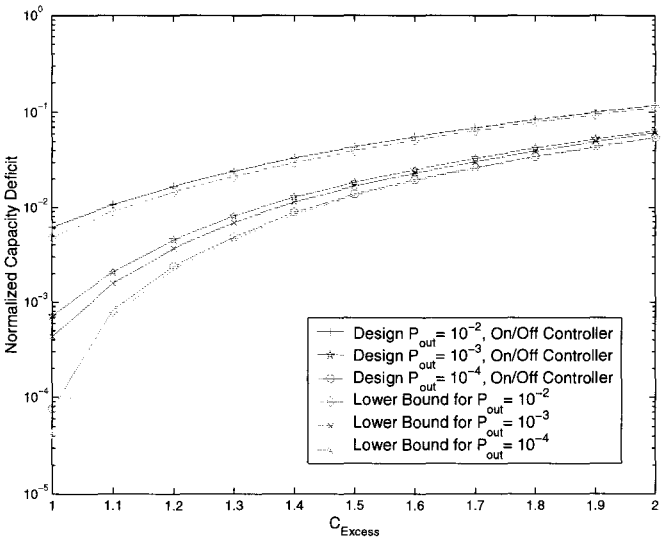

Figure 6.5: Capacity Deficit versus Excess Load (Control Algorithm Active).

by definition. In order to help characterize its performance we measure the minimum offered capacity and the length of time per year during which that capacity is offered. In Figure 6.8 this duration is shown for on/off control for different excess loading, where the minimum capacity is $\mathbf{U}_{min}$ and assuming $\mathbf{P}_{APmax}$ is 2W. Under on/off control the offered capacity takes on two values, 1 or $\mathbf{U}_{min}$. When proportional control is used this parameter is no longer discrete and can assume any value in the range, $[\mathbf{U}_{min}, 1]$. The corresponding graphs for the proportional/on/off control case is shown in Figure 6.9. It can be seen by comparing the two graphs that the time spent offering minimum capacity is much lower for the proportional/on/off controller compared with on/off control alone. This gives some additional indication that proportional/on/off control

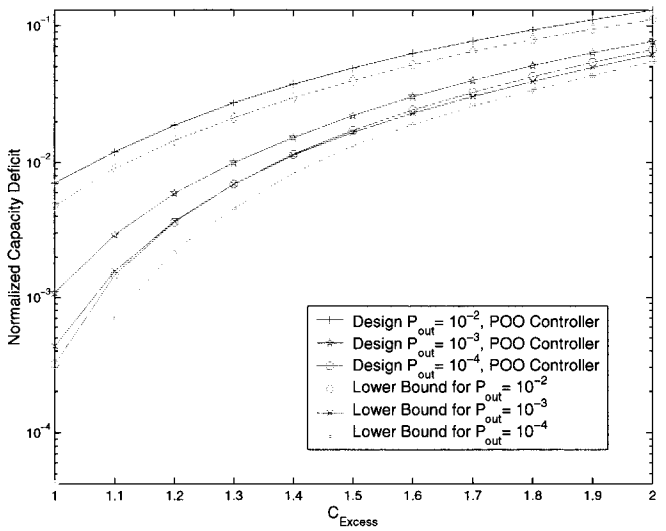

Figure 6.6: Capacity Deficit versus Excess Load (Proportional/On/Off Control)

is less abrupt in its capacity offering. For the 10^{-4} target outage case, Figure 6.9 shows that the proportional/on/off controller never offered capacity at the minimum value. Figure 6.10 also shows the actual minimum offered capacity as a function of excess load. It can be seen that in the higher outage design cases the minimum offered capacity drops very quickly to $\mathbf{U}_{min}$. However, in the 10^{-4} case the proportional control is enough to prevent that minimum level of offered capacity.

Figures 6.11 and 6.12 show the minimum capacity and its duration for different proportional control thresholds. As the control threshold is increased, the minimum offered capacity also increases since the controller is more ag-

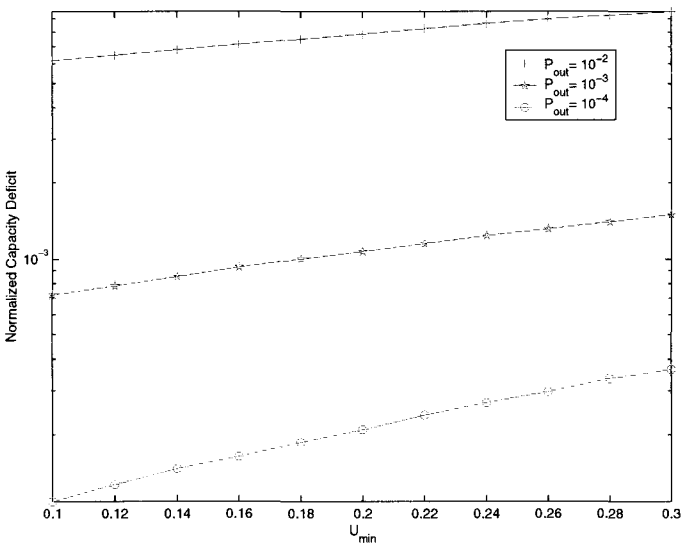

Figure 6.7: Capacity Deficit versus $\mathbf{U}_{min}$

gressively imposing a capacity deficit. For a design outage probability of 10^{-4}, the minimum offered capacity reaches 25%. At the same time, Figure 6.12 shows that the total duration that this minimum capacity is offered drops very quickly. These graphs suggest that if small amounts of capacity deficit are not critical, then it is best to choose large control thresholds.

6.4 Network Aware Design

So far, we used the proposed design methodology to design single nodes regardless of their involvement in an ESS mesh. In the single node design methodology, statistical knowledge of the traffic pattern in the node coverage area was considered in determining AOCP.

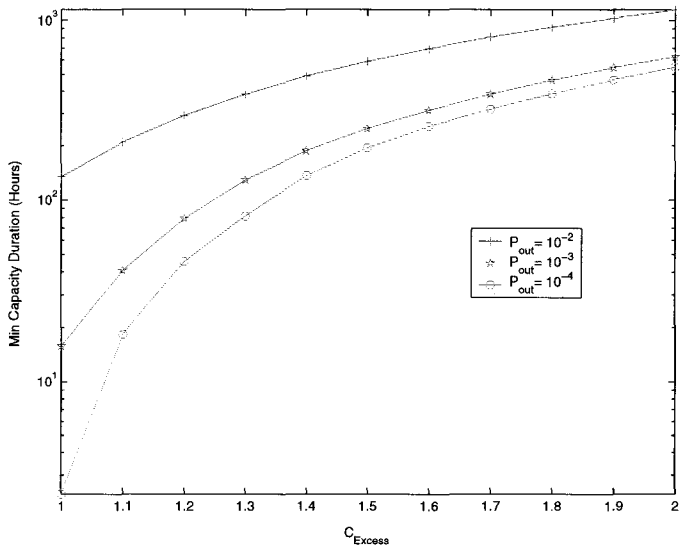

Figure 6.8: Duration of Minimum Offered Capacity (On/Off Control)

However, when an AP is a part of a mesh network it is not that straightforward to determine the expected AOCP. For every AP in a mesh network there are two types of traffic. The first type, the local traffic, is related to the end stations in the AP coverage area. The other one, the forwarding traffic, is the one that is coming from other MAPs or MPs. This latter one is dependent on the relative position of the AP in the mesh topology and the routing algorithm used.

In a tree topology, for example, with a sink at one of the nodes. Every AP is responsible of forwarding its own local traffic and the traffic coming from the nodes below it in the tree. When the topology is not a tree the routing algorithm determines which upper node must be used as the next hop. In practice, the most common mesh topology is a tree since the size of the ESS

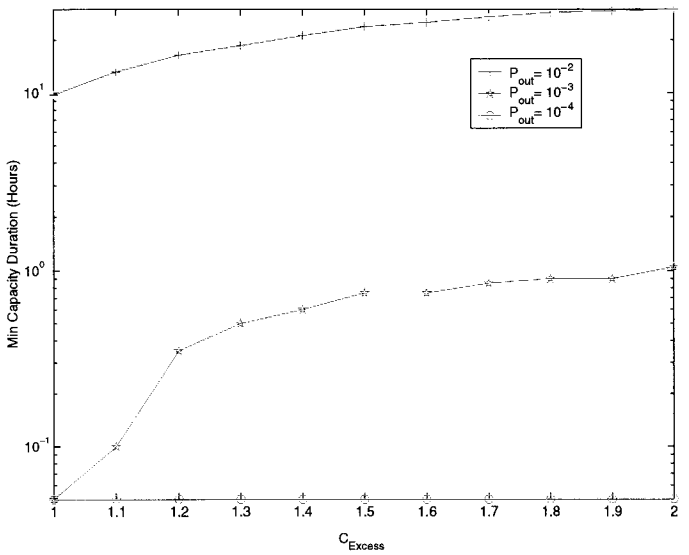

Figure 6.9: Duration of Minimum Offered Capacity (Proportional/On/Off Control)

mesh networks deployed for coverage extension rarely exceeds 5 or 6 nodes. In this section we consider a simple mesh topology and then based on the capacity allocation and the superframe management algorithms proposed in [21] the optimal sizing results are presented.

In Figure 6.13 we show an example of the type of architecture under consideration. AP_1 is AC powered while SMAPs 1-3 are solar powered. Each SMAP has two wireless cards; one for handling the incoming traffic, another for communicating with its parent in the tree. Again, we assume that $\mathbf{P}_{APmax}$ is 2W for the SMAPs and that $\mathbf{P}_{APmin}$ is 20mW.

As can be seen from the figure, $SMAP_1$ acts as a bottleneck in this topology

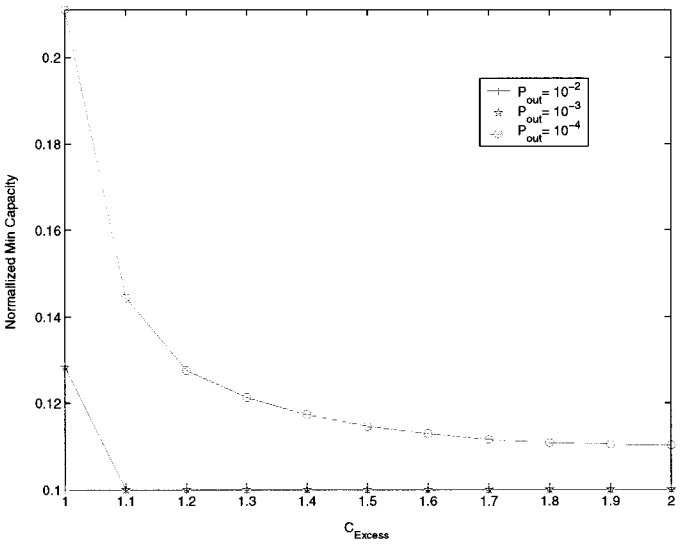

Figure 6.10: Minimum Offered Capacity for Proportional/On/Off Control

since all the traffic from $SMAP_2$ and $SMAP_3$ needs to go through it. We assume that the spatial distribution of the mobile users is uniform, meaning that each of the SMAPs is expected to handle the same amount of local traffic. On the wireless channel at frequency f_2 $SMAP_2$, $SMAP_3$ and the mobile stations associated with $SMAP_1$ are contending for transmission. A fair allocation of the capacity with respect to the uniform distribution of the users would be to grant a third of the available bandwidth to each of the above groups.

If this fairness is established, on the average any of the two lower SMAPs, $SMAP_2$ and $SMAP_3$, can at most offer 33% of the available capacity to their associated end stations. This constraint can be used in the statistical provisioning of the SMAP. We can write this as,

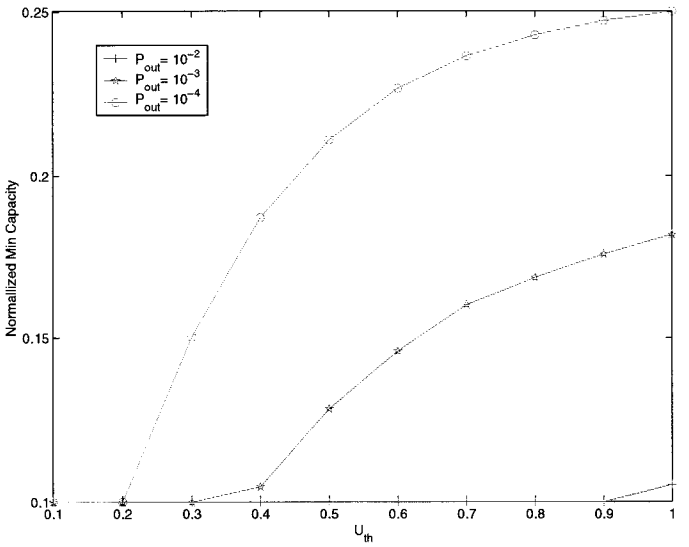

Figure 6.11: Minimum Offered Capacity for Proportional/On/Off Control

$$\texttt{AOCP}_{SMAP_2}(i) = \frac{1}{3}\,\texttt{AOCP}_{SMAP_1}(i). \tag{6.1}$$

Assuming full utilization at the bottleneck AP, we have $\texttt{AOCP}_{SMAP_2}(i) = \frac{1}{3}$. The optimum price panel and battery sizes for three outage probabilities are compared in the following table. It can be observed that by considering the topological constraints of an AP in a mesh network, significant reductions in system resources can be achieved. In Figures 6.14 and 6.15 contour plots for $\texttt{AOCP}_{SMAP_2}(\cdot)$ and $\texttt{AOCP}_{SMAP_1}(\cdot)$ are presented.

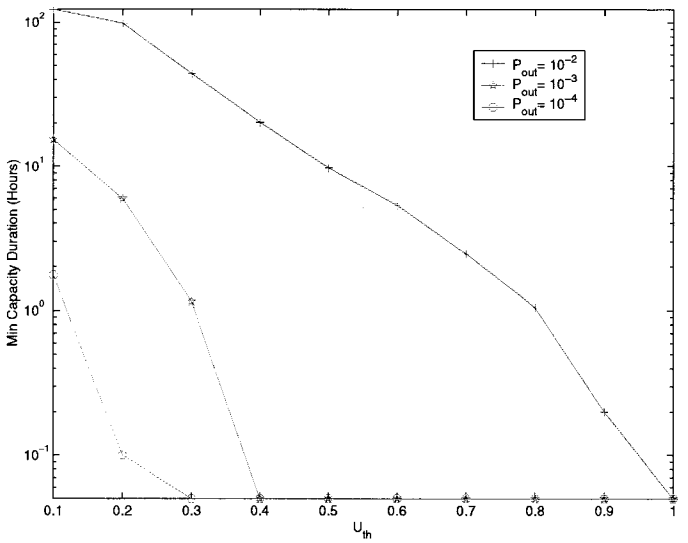

Figure 6.12: Time Duration of Minimum Capacity for Proportional/On/Off Control

	SMAP 1		SMAP 2	
$\mathbf{P}_{outage}$	$\mathbf{B}_{max}$	S_{pn}	$\mathbf{B}_{max}$	S_{pn}
10^{-2}	20.0	31.6	7.0	10.3
10^{-3}	30.1	38.0	9.2	13.0
10^{-4}	40.6	38.0	13.1	13.0

Table 6.2: Optimum Price Configurations for $SMAP_1$ and $SMAP_2$

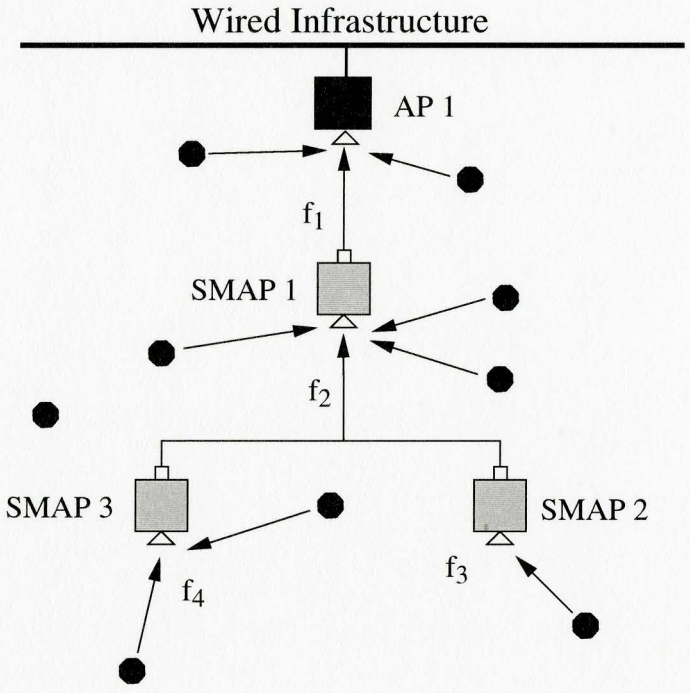

Figure 6.13: Example of Solar Powered ESS Mesh

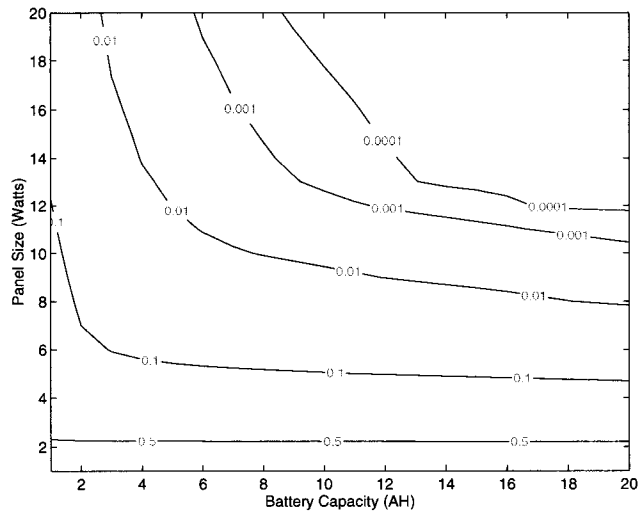

Figure 6.14: Outage Contour Plot for SMAP 2

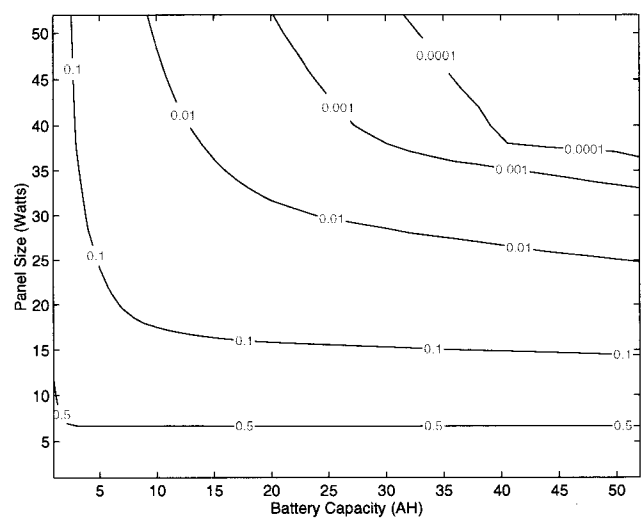

Figure 6.15: Outage Contour Plot for Node SMAP 1

Chapter 7

Conclusions and Future Research

The recent interest in wireless mesh networking has resulted in the need to sometimes deploy wireless APs in inaccessible places where the electrical power grid is not available. In SolarMesh networks, solar power is used to solve this problem and to make the wide-spread deployment of wireless mesh APs easier. However, the resource requirements and the energy provisioning of these solar-powered nodes highly depends on the AP's power consumption, which is an issue not originally of concern to the designers of the IEEE 802.11 standard.

In this thesis a design methodology and resource allocation scheme for solar powered IEEE 802.11 ESS mesh power saving infrastructure was proposed. This involves specifying a capacity profile which characterizes the workload that the AP will be designed to handle. Given a required reliability level and

averaged offered capacity profile, the system configuration is determined using available meteorological data.

The importance of ESS mesh power saving was demonstrated, and it was shown that significant reductions in system resources and node cost can be achieved by integrating power saving functionality into the APs. The performance result for different scenarios was presented to support these arguments. The proposed method, in general, can facilitate the wide-spread deployment of IEEE 802.11 ESS mesh networks because a large fraction of the total AP cost can be reduced by employing power-saving techniques in APs. However, in order to fully benefit from this, simple extensions to IEEE 802.11 are required.

The proposed design methodology is statistical, in that the nodes are designed for a target activity factor which may not be met in practice. For this reason a control algorithm was proposed which can reduce outage by dropping the offered capacity when needed. The effectiveness and performance of this control was characterized. It was shown that the algorithm can prevent outage even when loading greatly exceeds the design values. Proportional control was shown to more gracefully add capacity deficit to the system, and can result in larger minimum deficits.

In the past, it has always been assumed that energy is not an issue in wireless networking infrastructure. Therefore, many aspects of using limited or renewable energy sources in an ESS mesh network are not yet explored. Future research directions may include:

- Considering other types of renewable energy sources

  In some temperate climates similar to that of many places in Canada,

not much solar energy is available. Wind power can be considered as a strong alternative to solar energy.

- Application of solar power in sensor networks

  Sensor networks, due to their fundamental characteristics, are one of the best architectures where solar power can be used very effectively.

- More advanced control algorithms

  In the current control algorithms no differentiation is done between time-slots and the control algorithm makes the control decision regardless of the time of the day. Weights can be given to different time slots when the total capacity deficit is estimated.

Bibliography

[1] "The SolarMESH Network," 2004. http://owl.mcmaser.ca/solarmesh/.

[2] M. A. Abdelrahman and M. A. Elhadidy, ""Comparison of calculated and measured values of total radiation on tilted surfaces in Dhahran, Saudi Arabia"," *Solar Energy*, vol. 37, pp. 239–243, 1986.

[3] I. Abouzahr and R. Ramakumar, ""Loss of power supply probability of stand-alone photovoltaic systems: a closed form solution approach"," *Energy Conversion, IEEE Transactions on*, vol. 6, no. 1, pp. 1–11, 1991.

[4] P. Baikie, M. Gillibrand, and K. Peters, ""The effect of temperature and current density on the capacity of leadacid battery plates"," *Electrochimica Acta*, vol. 17, pp. 839–844, 1972.

[5] BelAir NEtworks Inc., "http://www.belairnetworks.com," 2005.

[6] B. S. Borowy and Z. M. Salameh, ""Optimum photovoltaic array size for a hybrid wind/PV system"," *Energy Conversion, IEEE Transactions on*, vol. 9, no. 3, pp. 482–488, 1994.

[7] M. Bouzguenda and S. Rahman, ""Energy management onboard the Space Station-a rule-based approach"," *Aerospace and Electronic Systems, IEEE Transactions on*, vol. 27, no. 2, pp. 302–310, 1991.

[8] L. L. Bucciarelli, ""Estimating loss-of power probabilities of stand-alone photovoltaic solar energy systems"," *Solar Energy*, vol. 32, no. 2, pp. 205–209, 1984.

[9] L. L. Bucciarelli, ""The effect of day-to-day correlation in solar radiation on the probability of loss of power in a stand-alone photovoltaic energy system"," *Solar Energy*, vol. 36, no. 1, pp. 11–14, 1986.

[10] C.-F. Chiasserini and R. Rao, ""Improving battery performance by using traffic shaping techniques "," *Selected Areas in Communications, IEEE Journal on*, vol. 19, no. 7, pp. 1385–1394, 2001.

[11] A. Ephremides, ""Energy concerns in wireless networks"," *Wireless Communications, IEEE*, vol. 9, no. 4, pp. 48– 59, 2002.

[12] A. Fragaki and T. Markvart, ""Does global warming affect the design of stand alone PV systems ?"," in *Solar-Wind-Hydrogen/Fuel Cells: Renewable Energies, Proc. 1st SWH International Conference*, pp. 155–56, 2003.

[13] U. Grasselli, ""Probabilistic design of high quality power supply photovoltaic systems"," in *Industrial and Commercial Power Systems Technical Conference, 1993. Conference Record, Papers Presented at the 1993 Annual Meeting*, 1993.

[14] HPWREN: High Performance Wireless Research and Education Network, "http://hpwren.ucsd.edu/solar.htmlh/." University of California, San Diego, CA.

[15] IEEE Standards Department, "802.11s ESS Mesh Networking working group," 2004.

[16] IEEE Standards Department, *Part 11: Wireless Medium Access Control (MAC) and Physical Laye r (PHY) specifications: Medium Access Control (MAC) Quality of Service (QoS) Enh ancements.* IEEE Press, 2005.

[17] C. E. Jones, K. M. Sivalingam, P. Agrawal, and J. C. Chen, ""A Survey of Energy Efficient Network Protocols for Wireless Networks"," *Wireless Networks*, vol. 7, no. 4, pp. 343–358, 2001.

[18] J. Jun and M. L. Sichitiu, ""The nominal capacity of wireless mesh networks"," *Wireless Communications, IEEE*, vol. 10, no. 5, pp. 8–14, Oct. 2003.

[19] A. Kansal and M. Srivastava, ""An environmental energy harvesting framework for sensor networks"," in *Low Power Electronics and Design, 2003. ISLPED '03. Proceedings of the 2003 International Symposium on*, pp. 481–486, 2003.

[20] S. A. Klein, ""Calculation of monthly average insolation on tilted surfaces"," *Solar Energy*, vol. 19, pp. 325–329, 1977.

[21] Y. Li, T. D. Todd, and D. Zhao, "Architecture and Protocols for Sustainable Solar-Powered ESS Mesh Networks," 2005.

[22] D. Macomber, ""Optimizing residential photovoltaic system size using approximate reasoning"," in *Uncertainty Modeling and Analysis,Proceedings., First International Symposium on*, pp. 558–563, 1990.

[23] H. Maghraby, M. Shwehdi, and G. Al-Bassam, ""Probabilistic assessment of photovoltaic (PV) generation system"," *Power Systems, IEEE Transactions on*, vol. 17, no. 1, pp. 205–208, 2002.

[24] M. Matsuda, ""Traffic information collection system powered by solar cells"," in *Intelligent Transportation Systems, 1999. Proceedings. 1999 IEEE/IEEJ/JSAI International Conference on*, pp. 870–873, 1999.

[25] Mesh Networks (Motorola Inc.), "http://www.meshnetworks.com," 2005.

[26] MeshDynamics Inc., "http://www.meshdynamics.com," 2005.

[27] MIT Roofnet, "http://www.pdos.lcs.mit.edu/roofnet/." Computer Science and Artificial Intelligence Laboratory, MIT, Cambridge, MA.

[28] C. Na and T. Rappaport, ""Measured wireless LAN public hotspot traffic statistics"," *Electronics Letters*, vol. 40, no. 19, pp. 1202– 1203, 2004.

[29] C. Na, J. Chen, and T. Rappaport, ""Hotspot traffic statistics and throughput models for several applications"," in *Global Telecommunications Conference, 2004. GLOBECOM '04. IEEE*, pp. 3257– 3263, 2004.

[30] L. Narvarte and E. Lorenzo, ""On the usefulness of stand-Alone PV Sizing Methods"," *Progress in Photovoltaics: Research and Applications, Prog.Photovolt: Res.Appl.*, vol. 8, pp. 391–409, 2000.

[31] National Climate Data and Information Archive, "http://www.climate.weatheroffice.ec.gc.ca/." The Meteorological Service of Canada, Canada., 2004.

[32] National Solar Radiation Data Base, "http://rredc.nrel.gov/solar/." National Renewable Energy Laboratory (NREL), U.S. Department of Energy, 2004.

[33] Nortel Networks, "http://www.nortelnetworks.com," 2005.

[34] R. Perez, P. Ineichen, R. Seals, J. Michalsky, and R. Stewart, ""Modeling daylight availability and irradiance components from direct and global irradiance"," *Solar Energy*, vol. 44, pp. 271–289, 1990.

[35] R. Perez, R. Seals, P. Ineichen, R. Stewart, and D. Menicucci, ""A New Simplified Version of the Perez Diffuse Irradiance Model for Tilted Surfaces"," *Solar Energy*, vol. 39, pp. 221–232, 1989.

[36] R. Perez and R. Stewart, ""Solar irradiance conversion models"," *Solar Cells*, vol. 18, pp. 213–222, 1986.

[37] A. Pesaran and V. Johnson, ""Battery Thermal Models for Hybrid Vehicle Simulations"," *Journal of Power Sources*, vol. 110, pp. 377–382, 2002.

[38] S. Saengthong and S. Premrudeepreechacham, ""A simple method in sizing related to the reliability supply of stand-alone photovoltaic systems"," in *Photovoltaic Specialists Conference, 2000. Conference Record of the Twenty-Eighth IEEE*, pp. 1630–1633, 2000.

[39] F. Safie, ""Probabilistic modeling of solar power systems"," in *Reliability and Maintainability Symposium, 1989. Proceedings., Annual*, pp. 425–430, 1989.

[40] Z. Salameh, M. Casacca, and W. Lynch, ""A mathematical model for lead-acid batteries"," *Energy Conversion, IEEE Transactions on*, vol. 7, no. 1, pp. 93–98, 1992.

[41] San Francisco BAWUG, "http://www.bawug.org/." San Francisco, CA.

[42] J. Schiller, A. Liers, H. Ritter, R. Winter, and T. Voigt, ""ScatterWeb - Low Power Sensor Nodes and Energy Aware Routing"," in *System Sciences, 2005. HICSS '05. Proceedings of the 38th Annual Hawaii International Conference on*, pp. 286– 286, 2005.

[43] Seattle Wireless, "http://www.seattlewireless.net/." Seattle, WA.

[44] S. Singh, M. Woo, and C. S. Raghavendra, ""Power-Aware Routing in Mobile Ad Hoc Networks"," in *MobiCom '98: Proceedings of the 4th annual ACM/IEEE international conference on Mobile computing and networking*, pp. 181–190, ACM Press, 1998.

[45] Southampton Open Wireless Network, "http://www.sown.org.uk/." Southampton, UK.

[46] C. K. Toh, ""Maximum battery life routing to support ubiquitous mobile computing in wireless ad hoc networks"," *Communications Magazine, IEEE*, vol. 39, no. 6, pp. 138 – 147, June 2001.

[47] R. van Drunen, J.Koolhaas, H.Schuurmans, and M.Vijn, ""Building a Wireless Community Network in the Netherlands"," in *USENIX/Freenix Conference*, pp. 219–230, 2003.

[48] T. Voigt, A. Dunkels, J. Alonso, H. Ritter, and J. Schiller, ""Solar-aware clustering in wireless sensor networks"," in *Computers and Communications, Proceedings. ISCC. Ninth International Symposium on*, pp. 238–243, 2004.

[49] T. Voigt, H. Ritter, and J. Schiller, ""Utilizing solar power in wireless sensor networks"," in *Local Computer Networks, Proceedings. 28th Annual IEEE International Conference on*, pp. 416–422, 2003.

[50] F. Zhang, T. D. Todd, D. Zhao, and V. Kezys, ""Power Saving Access Points for IEEE 802.11 Wireless Network Infrastructure"," in *IEEE Wireless Communications and Networking Conference 2004, WCNC'2004*, March 2004.